Journal of Pharmaceutical Analysis 13 (2023) 1526–1547

Contents lists available at ScienceDirect

Journal of Pharmaceutical Analysis

journal homepage: www.elsevier.com/locate/jpa

Original article

Gut dysbiosis aggravates cognitive deficits, amyloid pathology and lipid metabolism dysregulation in a transgenic mouse model of Alzheimer's disease

Chang Qu [a, b], Qing-Qing Xu [a], Wen Yang [a], Mei Zhong [a], Qiuju Yuan [c], Yan-Fang Xian [a, *], Zhi-Xiu Lin [a, d, **]

[a] School of Chinese Medicine, Faculty of Medicine, The Chinese University of Hong Kong, Hong Kong, China
[b] College of Forestry and Landscape Architecture, South China Agricultural University, Guangzhou, 510640, China
[c] Centre for Regenerative Medicine and Health, Hong Kong Institute of Science & Innovation, Chinese Academy of Sciences, Hong Kong Science Park, Shatin, N.T., Hong Kong, China
[d] Hong Kong Institute of Integrative Medicine, The Chinese University of Hong Kong, Hong Kong, China

ARTICLE INFO

Article history:
Received 26 March 2023
Received in revised form
22 July 2023
Accepted 25 July 2023
Available online 28 July 2023

Keywords:
Alzheimer's disease
Gut dysbiosis
Neuropathology
TgCRND8 mice

ABSTRACT

Gut dysbiosis, a well-known risk factor to triggers the progression of Alzheimer's disease (AD), is strongly associated with metabolic disturbance. Trimethylamine *N*-oxide (TMAO), produced in the dietary choline metabolism, has been found to accelerate neurodegeneration in AD pathology. In this study, the cognitive function and gut microbiota of TgCRND8 (Tg) mice of different ages were evaluated by Morris water maze task (MWMT) and 16S rRNA sequencing, respectively. Young pseudo germ-free (PGF) Tg mice that received faecal microbiota transplants from aged Tg mice and wild-type (WT) mice were selected to determine the role of the gut microbiota in the process of neuropathology. Excessive choline treatment for Tg mice was used to investigate the role of abnormal choline metabolism on the cognitive functions. Our results showed that gut dysbiosis, neuroinflammation response, Aβ deposition, tau hyperphosphorylation, TMAO overproduction and cyclin-dependent kinase 5 (CDK5)/transcription 3 (STAT3) activation occurred in Tg mice age-dependently. Disordered microbiota of aged Tg mice accelerated AD pathology in young Tg mice, with the activation of CDK5/STAT3 signaling in the brains. On the contrary, faecal microbiota transplantation from WT mice alleviated the cognitive deficits, attenuated neuroinflammation, Aβ deposition, tau hyperphosphorylation, TMAO overproduction and suppressed CDK5/STAT3 pathway activation in Tg mice. Moreover, excessive choline treatment was also shown to aggravate the cognitive deficits, Aβ deposition, neuroinflammation and CDK5/STAT3 pathway activation. These findings provide a novel insight into the interaction between gut dysbiosis and AD progression, clarifying the important roles of gut microbiota-derived substances such as TMAO in AD neuropathology.

1. Introduction

As the most common form of neurodegenerative disease, Alzheimer's disease (AD) affects approximately 50 million people worldwide. And AD incidence was projected to grow substantially in the coming decades [1]. Aging-associated cognitive dysfunction is a major risk factor for AD, which is consistent with the fact that a large majority of AD cases are reported in older adults. Among people aged over 85, more than one-third develop AD [2]. The rapidly aging population worldwide has exacerbated this issue and heightened the need for effective interventions for AD.

A number of age-associated changes in functionality and pathological alterations have been identified in AD. Aggregated extracellular β-amyloid (Aβ) plaques, intraneuronal neurofibrillary tangles (NFTs), and loss of neurons with age have been observed in both rodents and humans. NFTs are composed of microtubule-associated protein tau. Although neuronal death, tangles, and pathological plaques are commonly observed in AD cases, the mechanistic interaction between these traits and AD neurological damage has not been clearly clarified. Among these, cyclin-

Peer review under responsibility of Xi'an Jiaotong University.
* Corresponding author.
** Corresponding author. School of Chinese Medicine, Faculty of Medicine, The Chinese University of Hong Kong, Hong Kong, 000000, China.
E-mail addresses: lisaxian@cuhk.edu.hk (Y.-F. Xian), linzx@cuhk.edu.hk (Z.-X. Lin).

https://doi.org/10.1016/j.jpha.2023.07.014

dependent kinase 5 (CDK5) has been found to play a decisive role in the AD progression. CDK5 can be activated by its activators p35 and p39 (or their respective reduced forms, p25 and p29). Abnormality of the CDK5/p25 complex promotes excessive hyperphosphorylation of CDK5 substrates, then triggers AD [3]. Therefore, CDK5 activation is considered to increase Aβ deposition in both the neurites and neuronal cell body [4], while inhibition of CDK5 activity significantly attenuates Aβ accumulation in those transgenic mice that over-express p25 [5]. During the process of CDK5 activation, signal transducer and activator of transcription 3 (STAT3), a substrate of CDK5/p25, functions as a key transcription factor [6]. In addition, tyrosine phosphorylation of STAT3 participates in modulating the transcriptional activity of STAT3. Previous work proved that the phosphorylated STAT3 was markedly elevated in the brains of amyloid precursor protein/presenilin 1 (APP/PS1) transgenic mice, also in the neurons treated with Aβ. In contrast, suppression of STAT3 activation can notably attenuate Aβ-induced neuronal cell death [7]. Most importantly, CDK5 was proven to mediate STAT3 phosphorylation, enhance the transcriptional activity of STAT3, resulting in the elevated transcription of BACE1, and finally increase the Aβ accumulation [3]. Hence, there is obviously a feedback loop between Aβ and neuropathology via the CDK5/STAT3 signalling pathway activation.

Over the past decades, although extensive efforts have been made to unravel the molecular mechanisms underlying AD etiopathogenesis, majority still remains incompletely understood. In recent years, emerging evidence indicates that gut dysbiosis affects except the composition and physiological function of the gut, influences the cognitive function of host, and potentially augments the incidence of AD progression [8]. Actually, gut microbiota interacts with the central nervous system (CNS), regulates brain functions and influences behavioural performance via the bidirectional microbiota-gut-brain axis. Previous research indicated that the diversity and composition of gut bacteria in AD patients were markedly different from those in healthy controls [9]. Additionally, gut microbes influence host metabolism by metabolising dietary and host-derived substrates, including synthesizing neurotransmitters such as γ-aminobutyric acid, modulating systemic immune cells and producing metabolites such as short-chain fatty acids, all of which have important implications for neurodegenerative disorders [10].

However, the mechanistic link among the gut microbiota, microbiota-derived metabolites and the associated deteriorations in cognitive function in AD is still undefined. Therefore, we here analyzed the gut microbiota of TgCRND8 mice (transgenic AD model mice, Tg) using 16S rRNA sequencing and their plasma samples using untargeted metabolomics profiling to explore whether the cognitive deficits in aging Tg mice with age are associated with the changes in and interactions of the gut microbiota and its derived metabolites. We also performed faecal microbiota transplantation (FMT) and excessive choline treatment to verify the pivotal roles of the gut microbiota and lipid metabolism in cognitive deficits, neuroinflammation, tau hyperphosphorylation and Aβ deposition in Tg mice. Tg mouse, a heterozygous transgenic mouse, expressing two human APP695 mutations such as Swedish (K670 N/M671L) and Indiana (V717F) with the background of C57BL/6 F3 [11], were used in the study to breed a colony of experimental with AD. Aβ deposits were observed in 3-month-old Tg mouse in its hippocampal and cortical areas, accompanied by the activation of astrocyte and microglia, inflammation, neuritic dystrophy, and cognitive deficits. These pathological characteristics closely resemble the AD pathology in clinic [11]. The clarification of the mechanisms underlying the neuro-regulation by gut microbiota may provide a novel perspective for developing effective targets for AD therapy.

2. Materials and methods

2.1. Materials

Anti-IBA-1 antibody was obtained from Wako Biotechnology (Richmond, VA, USA). $A\beta_{40}$ and $A\beta_{42}$ enzyme-linked immunosorbent assay (ELISA) kits were purchased from Invitrogen (Grand Island, NY, USA). Tumor necrosis factor-α (TNF-α) ELISA kits were obtained from Raybiotech (Norcross, GA, USA). Interleukin-1β (IL-1β) and interleukin-6 (IL-6) ELISA kits were purchased from Abcam (Cambridge, UK). Radioimmunoprecipitation assay buffer (RIPA), protease/phosphatase inhibitor cocktail, PierceTM ECL western blotting substrate, and interleukin-17 (IL-17) ELISA kits were bought from Thermo Fisher Scientific (Waltham, MA, USA). Anti-β-amyloid 17–24 antibody, anti-GFAP polyclonal antibody, ampicillin, neomycin, metronidazole, choline, and all other reagents were provided from Sigma-Aldrich (St. Louis, MO, USA).

2.2. Animals

Tg mice with the (C57BL/6J) × (C3H/HeJ × C57BL/6J) genetic background were bred in a specific-pathogen free animal breeding room in the Laboratory Animal Services Centre of The Chinese University of Hong Kong (CUHK), and maintained in a humidity (50% ± 10%) and temperature-controlled (22 ± 2 °C) on a 12 h light/dark cycle with ad libitum access to food and water. Before the formal experiments, all mice were subjected to genotyping to detect the APP transgene type based on our previous studies [12,13]. Then, male Tg mice and their non-transgenic wild-type (WT) littermates with different ages (2, 4, 6, 8, 10 and 12 months, respectively) were identified and randomly distributed to the experimental groups (Fig. 1A). 3-month-old male Tg mice were used in the subsequent FMT treatment experiment and excessive choline experiment. All mice were housed in a group with 4–5 mice per cage before collecting the fecal samples for gut microbiota analysis. The mice were put into a clean cage when the fecal samples were collected, and the fecal samples were collected with sterile forceps and put into a centrifuge tube immediately to avoid too long oxygen exposure-drying of fecal matter. Two investigators who were blinded to the group distribution measured the behavioural tests. All experimental protocols of the whole study have obtained the approval (Approval number: 19/096/GRF-4-B) from the Animal Experimentation Ethics Committee of CUHK.

2.3. FMT treatment experiment

Three-month-old male mice were divided into 4 groups as WT group, Tg group, Tg + WT-FMT group and Tg + Tg-FMT group ($n = 8$/groups). Antibiotic cocktail (ABX) was composed of ampicillin (2.5 g/L), neomycin (1.25 g/L) and metronidazole (2.5 g/L). All mice were orally administered with ABX for consecutive 5 days to establish pseudo-germ-free (PGF) models based on previous research with minor modification [14,15]. Daily dosage of ABX for each mouse was 0.2 mL. During the antibiotic treatment period, stools were collected for real-time checking of dynamic changes of gut microbiota to ensure that the gut microbiome was eliminated. Low quantities of total DNA and bacterial diversity in stools from mice indicated that PGF model had been successfully established after ABX treatment for 5 consecutive days. On day 6, mice in the Tg + Tg-FMT and Tg + WT-FMT groups were intragastrically administered with fresh faecal solution (0.2 mL) once daily for 10 consecutive weeks. Specifically, fresh faecal samples were daily collected from 10-month-old Tg and age-matched WT mice, mixed

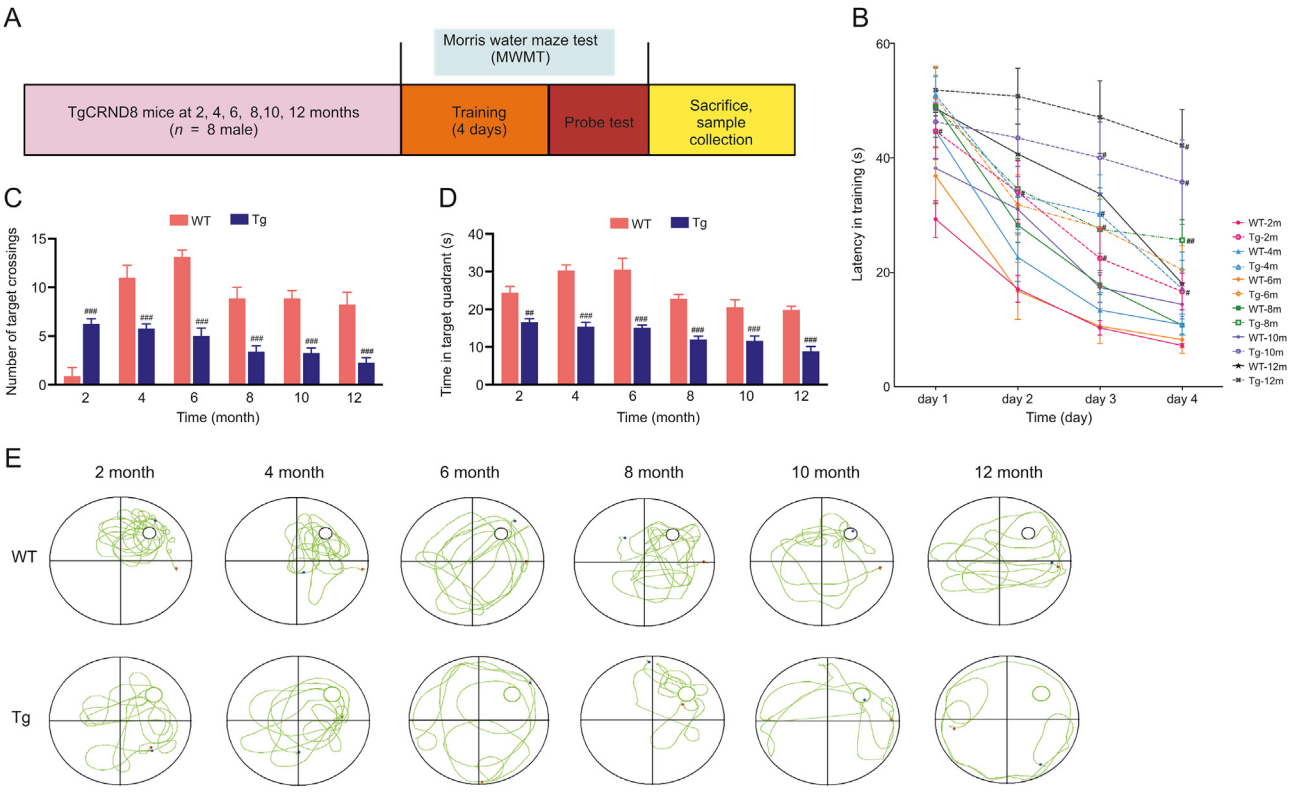

Fig. 1. Cognitive deficits are aggravated in an age-dependent manner in TgCRND8 (Tg) mice. (A) Schematic diagram of the experimental design. (B) Escape latency of mice for 4 consecutive days in the Morris water maze task (MWMT). (C) Number of target crossing of the mice in the probe test of the MWMT. (D) Time spent in the target quadrant in the probe test of the MWMT. (E) Representative swimming tracks of mice in the MWMT. Data are presented as the mean ± standard error mean (SEM) ($n = 8$). $^{\#}P < 0.05$, $^{\#\#}P < 0.01$, $^{\#\#\#}P < 0.001$ compared with the wild-type (WT) group.

with the sterile normal saline (0.1 g/mL) and then homogenised for 2 min. Then, the faecal materials were prepared by sonicating for 3 min and centrifugated at 6000 *g*, and 4 °C for 15 min. The obtained faecal suspension was used for intragastrically administered to mice in Tg + Tg-FMT and Tg + WT-FMT. For the same duration, mice in WT group and Tg group were intragastrically administered with the same volume of 0.9% saline, and the feeding and environmental condition were consistent for all mice. At the end of FMT treatment, all the mice were subjected to the Morris water maze test (MWMT) and open-field test (OFT).

2.4. Excessive choline treatment experiment

The dose of choline in this study was chosen according to the literature with modifications [16]. Women and men were recommended to intake 425–550 mg of choline per day. In this study, 500 mg/60 kg/day was considered as the daily recommended dose of choline for humans. Accordingly, 15 times of the normal daily dose, i.e., 7500 mg/60 kg/day, was considered as an excessive choline dose for humans. This excessive dose for humans was converted into an excessive dose for mice using the following parameters: an adult of 60 kg with a conversion factor of 9 between human and mouse yields an excessive dose of 1 g choline/kg/day for mice.

Three-month-old male mice were randomly distributed into three groups: WT group, Tg group and Tg + choline group. Mice were daily intragastrically administered with choline (1 g/kg, dissolved in 0.9% saline) for 3 months in the Tg + choline group. For the same duration, mice in WT and Tg groups were intragastrically administered with the same volume of 0.9% saline and the feeding and environmental condition were consistent for all mice. At the end of choline treatment, mice were subjected to MWMT and OFT.

2.5. MWMT

The MWMT was performed as previously described [12,13]. The modular MWMT with the video tracking software SuperMaze V2.0 was designed by Xinruan Information Technology Co. Ltd. (Shanghai, China). A circular tank (150 cm diameter and 70 cm height) was filled with 25 °C water. The tank was separated into four equal quadrants with various prominent shapes including triangles, circles, stars and quadrangles. A circular escape platform with 10 cm diameter was put in the middle of a quadrant and hidden 2 cm below the water's surface. In the first consecutive 4 days, mice were trained to find the hidden platform. Each mouse was daily trained for three trials with an interval of 60 s between consecutive trials. In each trial, mice were mildly placed in a specific quadrant with their nose pointing toward the wall. Then each mouse was free to find the escape platform for 60 s and stay on it for 30 s. If the mouse couldn't find the hidden platform within 60 s, it was put on the platform for 30 s, and the escape latency (finding the hidden platform) was written down as 60 s. To measure the spatial learning ability, the time of mouse spent on reaching the platform was recorded. On day 5, we conducted a probe test by removing the hidden platform to evaluate the spatial memory of mice. The number of target crossings and the time spent in the target quadrant were recorded. During the duration, the MWMT was conducted from 9:00 to 18:00 every day to eliminate the differences caused by circadian rhythmicity.

2.6. OFT

OFT was used to evaluate the locomotor activity of rodents [17,18]. A box (50 cm × 50 cm × 60 cm) with white floor separated

into 16 equal squares acted as an open field. Mice were subjected totraining on day 1 and then testing on day 2. The total distance traveled and the time spent in the central area of the field were recorded to evaluate the exploratory behaviour and locomotor activity of mice, respectively. Each trial lasted 10 min. Between each trial, the box was swept with 10% aqueous ethanol solution to minimize the influences of the smell from previous mice.

2.7. Gut microbiota analysis

To avoid genomic DNA contamination, faecal samples for gut microbiota analysis were treated with DNase (4U; DNA-free, Ambion) with RNase inhibitor (RnaseOut, Invitrogen Life Technologies) for 1 h at 37 °C before DNA extraction. DNA was isolated using the hexadecyltrimethylammonium bromide/sodium dodecyl sulfate method from stool samples ($n = 6$/group). The purity and concentration of DNA samples were measured using 1% agarose gels. The DNA samples were diluted with sterile water to 1 ng/μL and subjected to polymerase chain reaction (PCR) for the amplification of 16S rRNA genes using a complex of forward and reverse primers with a unique 12-base barcode for labeling PCR products from each sample. The sequencing of paired-end 16S community was then performed on an Illumina platform by the bacterial/archaeal primers 341F/806R, which were specific for the V3-4 region of the 16S rRNA gene. All PCR cycles were performed out in the reaction mixtures (30 μL) containing around of template DNA (10 ng), Phusion®High Fidelity PCR Master Mix (15 μL) (New England Biolabs, Ipswich, MA, USA), and a mixture of a forward primer and a reverse primer (0.2 μM). The thermal cycling reactions were performed at 98 °C for 1 min, followed denaturation by 30 cycles at 98 °C for 10 s, annealing for 30 s at 50 °C and elongation for 60 s at 72 °C, and then final extension of 5 min at 72 °C. Samples with a bright main strip at 400–450 bp were chosen for the following experiments. PCR products were mixed in the ratio of isodense, and then purified with an AxyPrepDNA Gel Extraction Kit. The sequencing libraries were created with an NEB Next®Ultra™DNA Library Prep Kit for Illumina (New England Biolabs) per the manufacturer's instructions, and added the index codes. The quality of the library was evaluated using the Agilent Bioanalyzer 2100 system and a Qubit@ 2.0 Fluorometer (Thermo Scientific). Finally, the library was sequenced on an Illumina HiSeq2500 platform, and generated with 250-bp/300-bp paired-end reads.

The STAMP software was used to determine the differences in the abundances of individual taxa between different groups. The quantitative of biomarkers within different groups were analyzed using linear discriminant analysis effect size (LEfSe) analysis. LEfSe was used to analyze the species, the number of which is much higher than that of samples, and to afford the biological consistency class, and effect size estimation of predicted biomarkers. To identify differences in the microbial community composition between different groups, an analysis of similarities (ANOSIM) and a permutational multivariate analysis of variance (ADONIS) were conducted according to the Bray-Curtis dissimilarity distance matrices.

2.8. Protocol for untargeted metabolomic profiling

Blood samples were harvested using Eppendorf tubes containing heparin sodium (1%) and centrifuged for at 4,000 rpm for 20 min at room temperature. Afterward, the plasma samples were collected and thawed at 4 °C. In order to deproteinization, 100 μL of each plasma sample was added with cold methanol/acetonitrile (400 μL, 1:1, *V/V*). After that, the reaction solution was centrifuged at 14,000×*g* for 15 min at 4 °C, and the obtained supernatant was dried by vacuum centrifuge. Finally, the residues were dissolved in acetonitrile: water (100 μL, 1:1, *V/V*) solvent for the ultra-high-performance liquid chromatography-quadrupole time-of-flight with mass spectrometry (UHPLC/Q-TOF/MS) analysis.

2.9. UHPLC-Q-TOF/MS analysis

Metabolomic analysis was conducted with a UHPLC system (1290 Infinity LC, Agilent Technologies) and quadrupole time-of-flight detector (AB Sciex Triple TOF 6600, Mundelein, IL, USA). ACQUITY UPLC BEH column (2.1 mm × 100 mm, 1.7 μm; Waters, Milford, MA, USA) was used in UHPLC analysis. The amount of samples (2 μL) was injected into the automatic sampler at 4 °C and the flow rate was set at 0.5 mL/min. The separated temperature was stayed at 25 °C. The mobile phase was composed of the water containing ammonium acetate (25 mM) and ammonium hydroxide (25 mM) (solution A) and acetonitrile (solution B). During the chromatography run, the gradient was 95% B for 0.5 min, linearly declined to 65% with 7 min and further to 40% with 1 min, followed by keeping for 1 min. Finally, the gradient was enhanced to 95% with 0.1 min and the column was re-equilibrated over 3 min.

2.10. Principal component analysis (PCA)

PCA analysis was conducted using quantitative data by SIMCA (Version 14.1) obtained from high-throughput sequencing of 16S rRNA analysis and metabolomics by LC/MS analysis.

2.11. Kyoto Encyclopedia of Genes and Genomes (KEGG) pathway analysis

All differential metabolites were mapped to pathways by online KEGG (http://www.kegg.jp/). KEGG annotation and enrichment results of high-throughput sequencing by 16S rRNA analysis and metabolomics from UHPLC-Q-TOF/MS analysis were combined by R (Version 3.5.1). Also, bar plots and venn diagrams were depicted.

2.12. Correlation analysis

Differentially abundant metabolites were log2 scaled (TMT/iTRAQ) and concatenated into one matrix. Subsequently, correlation coefficients among all molecules in the matrix were calculated using the Pearson algorithm in R (Version 3.5.1).

2.13. Correlation network

Pearson's correlation coefficients between the distinctly expressed genes/proteins/modified peptides and lipids/metabolites were uploaded to CytoScape (Version 3.5.1), and the relative correlation network was computed.

2.14. Brain sample processing

After the behavioural tests, 6 mice of each group were sacrificed under anaesthesia. The brain tissues were harvested and divided into two equal parts for further ELISA kits and western blotting analyses. For immunofluorescence (IHC) analysis, mice (4/group) were deeply anaesthetised and perfused with cold saline (0.9%) through hearts, following by fixing in 4% paraformaldehyde. Then the brain tissues were post-fixed in 4% paraformaldehyde at 4 °C for overnight. Finally, the tissues were kept at 4 °C in 30% sucrose solution until sectioning.

2.15. $A\beta_{40}$ and $A\beta_{42}$ ELISA kits

100 mg brain tissues were homogenised in cold lysis buffer (5 M guanidine-HCl:50 mM Tris, pH 8.0) with protease inhibitor cocktail (1%). The homogenates were blended using an orbital shaker at 25 °C for 4 h, and then centrifuged for 20 min at 16,000 *g*, 4 °C. The obtained supernatants were analyzed by mouse $A\beta_{40}$ and $A\beta_{42}$ ELISA kits per the manufacturer's guidance. The concentrations of $A\beta_{40}$ and $A\beta_{42}$ were determined by calculating with the standard curves.

2.16. Cytokine determination and trimethylamine N-oxide (TMAO) measurement

The brain and colon tissues were homogenised thoroughly in lysis buffer (provided by ELISA kits), incubated on ice for 20 min, and then centrifuged for 20 min at 12,000 rpm, 4 °C. The concentrations of TNF-α, IL-6, IL-1β, IL-17 and TMAO in the obtained supernatants were measured by ELISA kits per the manufacturer's guidance.

2.17. Western blotting

Firstly, brain tissues of mice were lysed in RIPA buffer containing protease/phosphatase inhibitor cocktail (1%) and centrifuged for 15 min at 14,000 rpm, 4 °C to obtain the protein samples. Equal amounts of proteins from different groups were added into polyacrylamide gel. After separated using polyacrylamide gel electrophoresis with sodium dodecyl sulfate, the samples were shifted into PVDF membranes. The intensity of each band was imaged using Acer c300 (Azure Systems, Mumbai, India) and analyzed using ImageJ software (NIH Image, Bethesda, MD, USA).

2.18. IHC assay

Brain tissues were cut into 30 μm slices by cryostat (Leica CM1850, Leica Microsystems GmbH, Wetzlar, Germany) and stored at 4 °C in phosphate buffered saline (PBS, 0.1 M). Then the slices were steeped in 0.25% trypsin and incubated for 30 min at 37 °C for antigen retrieval before staining. After that, the slices were rinsed in PBS three times, for 15 min each time, followed by permeabilisation in PBS solution containing 0.3% Triton, and finally incubated overnight on a shaker at 25 °C in a blocking solution containing primary antibodies such as anti-β-amyloid 17–24, anti-GFAP and anti-IBA-1. After overnight incubation, the slices were washed with PBS three times for 15 min per time and incubated with relative secondary antibodies (1:500) for 2 h at room temperature. The sections were then rinsed with PBS three times for 15 min each time, then mounted with fluorescence mounting medium (Dako North America, Inc., CA, USA) and covered with a coverslip. The immunofluorescent images were captured by Zeiss fluorescent inverted microscope (Zeiss, Göttingen, Germany). The fluorescence was quantified with ImageJ software (NIH Image, Bethesda, MD, USA).

2.19. Statistical analysis

All data are presented as the mean ± standard error mean (SEM). Inter-group differences of the escape latency in the MWMT were analyzed using a two-way repeated measures analysis of variance (ANOVA), with the factors being treatments and training days. The inter-group differences of the other data were analyzed using a one-way ANOVA followed by post-hoc Bonferroni's test. Group differences between two groups were analyzed using Student's *t*-test. All statistical analyses were performed using GraphPad Prism software (Version 8, GraphPad Software, Inc., La Jolla, CA, USA). When *P* value was less than 0.05, it was deemed statistically significant.

3. Results

3.1. Cognitive deficits were aggravated in Tg mice in an age-dependent manner

To evaluate the cognitive function of Tg mice at different ages, we trained the mice to find the hidden platform in the MWMT. In the training trials, mice of all groups learned to find the hidden platform, and the escape latency to find the platform shortened with increasing age. Significant differences were observed in the mean latency during the training period, specifically, on day 1, 2 and 3, 2-month-old Tg mice exhibited longer escape latencies (day 1: T = 2.811, day 2: T = 2.498, day 3: 2.976) than their age-matched WT littermates (all $P < 0.05$). On day 3, 4-, 6- and 10-month-old Tg mice exhibited longer escape latencies (T = 2.532, 2.601 and 2.917, respectively) than their WT littermates with similar ages (all $P < 0.05$). On day 4, 2-, 8-, 10- and 12-month-old Tg mice exhibited longer escape latencies (T = 2.810, 3.875, 2.947 and 2.928, respectively) than their age-matched WT littermates (all $P < 0.05$) (Fig. 1B). Also, remarkable differences were inspected in the number of times mice crossed the platform quadrant in the MWMT between Tg mice and WT mice aged 2 months (T = 4.512, $P < 0.001$), 4 months (T = 4.407, $P < 0.001$), 6 months (T = 6.820, $P < 0.001$), 8 months (T = 4.617, $P < 0.001$), 10 months (T = 4.722, $P < 0.001$) and 12 months (T = 5.036, $P < 0.001$) (Fig. 1C). Furthermore, prominent differences were found in the time spent in the target quadrant between Tg mice and WT mice aged 2 months (T = 3.537, $P < 0.01$), 4 months (T = 6.990, $P < 0.001$), 6 months (T = 7.219, $P < 0.001$), 8 months (T = 4.899, $P < 0.001$), 10 months (T = 4.158, $P < 0.001$) and 12 months (T = 4.963, $P < 0.001$) (Fig. 1D). The above results demonstrate that spatial learning and memory deficits occurred in the Tg mice. Representative swimming paths of mice are illustrated in Fig. 1E.

3.2. Neuroinflammation was activated in the brains of Tg mice in an age-dependent manner

To examine whether cognitive dysfunction is related to chronic neuroinflammation in mice, as observed in AD pathology in humans, we conducted immunohistochemical (IHC) staining of brain tissues from WT and Tg mice of different ages. As shown in Figs. 2A and 3A, the co-staining of Aβ/IBA-1 and Aβ/GFAP revealed significant differences in the accumulation of IBA-1-positive microglia between Tg mice and WT mice aged 2 months (T = 3.317, $P < 0.05$), 4 months (T = 4.729, $P < 0.001$), 6 months (T = 5.435, $P < 0.001$), 8 months (T = 6.211, $P < 0.001$), 10 months (T = 6.494, $P < 0.001$) and 12 months (T = 8.752, $P < 0.001$). The co-staining also revealed significant differences in the accumulation of GFAP-positive astrocytes between Tg mice and WT mice aged 4 months (T = 5.198, $P < 0.001$), 6 months (T = 5.268, $P < 0.001$), 8 months (T = 7.278, $P < 0.001$), 10 months (T = 8.872, $P < 0.001$) and 12 months (T = 8.1779, $P < 0.001$). These results indicate that activation microglia and astrocytes were markedly gathered around the Aβ plaques in Tg mice in an age-dependent manner. Notably, Aβ plaques were also sharply accumulated in Tg mice with increasing age. Significant differences were observed in Aβ plaque accumulation between Tg mice and WT mice aged 2 months (T = 5.692, $P < 0.001$), 4 months (T = 7.969, $P < 0.001$), 6 months (T = 14.17, $P < 0.001$), 8 months (T = 19.14, $P < 0.001$), 10 months (T = 26.18, $P < 0.001$) and 12 months (T = 31.84, $P < 0.001$) (Figs. 2B and 3B). These observations were consistent with the $A\beta_{40}$ and $A\beta_{42}$ concentrations measured in the

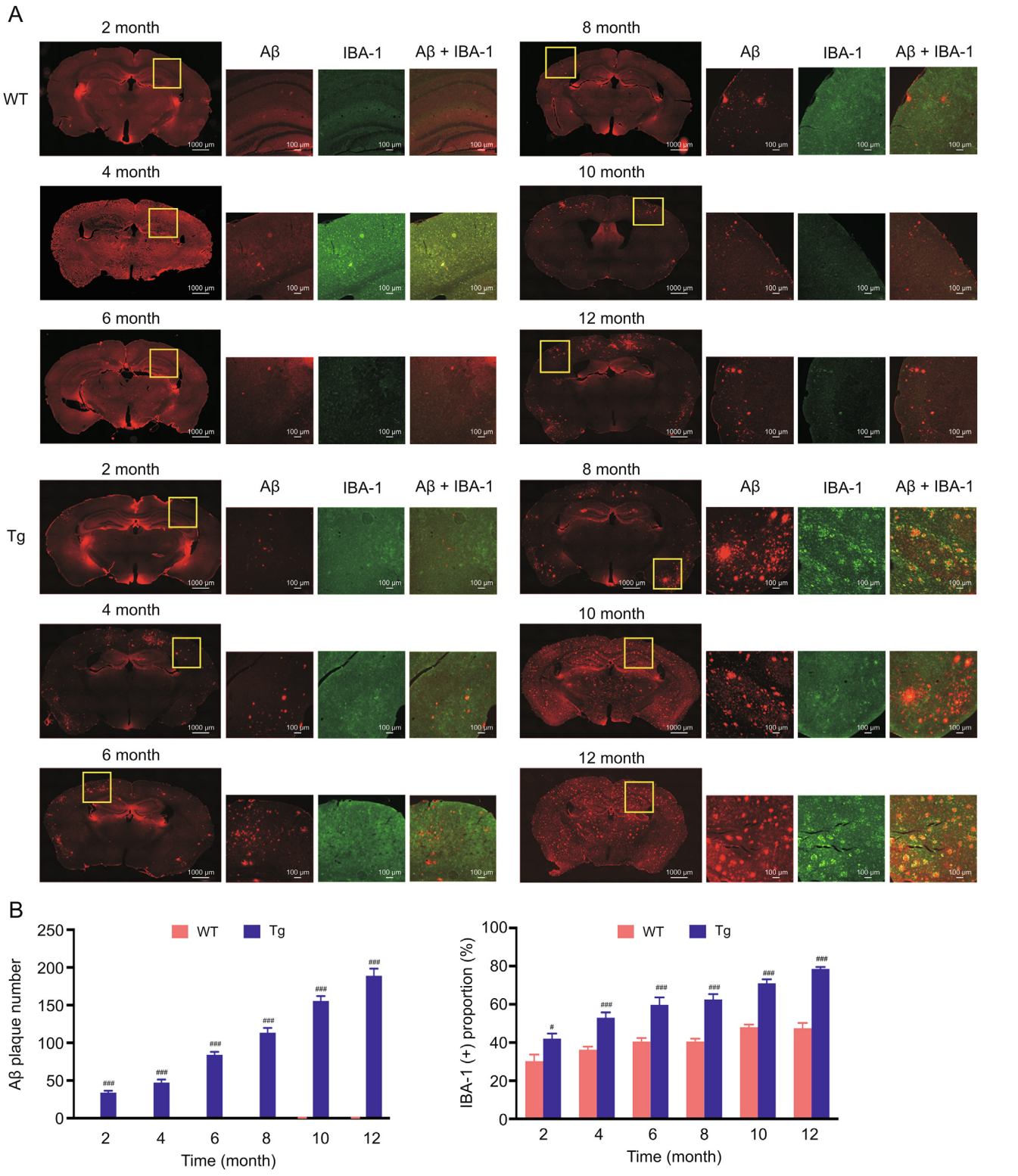

Fig. 2. Activation of microglia is elevated in an age-dependent manner in the brain tissues of TgCRND8 (Tg) mice. (A) Immunohistochemistry (IHC) co-staining of amyloid beta (Aβ)/IBA-1 co-staining in the brain tissues of Tg and wild-type (WT) mice. (B) Quantitative analysis of IHC staining. Data are presented as the mean ± standard error mean (SEM) ($n = 4$). $^{\#}P < 0.05$ and $^{\#\#\#}P < 0.001$ compared with the WT group (t-test).

brains of Tg mice (Fig. 4A). Overall, these findings suggest that with aging, inflammatory responses were stronger in the brains of Tg mice than in those of their WT littermates.

Significant differences were observed in the concentration of $A\beta_{40}$ between Tg mice and WT mice aged 2 months (T = 4.356, $P < 0.01$), 4 months (T = 5.008, $P < 0.001$), 6 months (T = 7.297, $P < 0.001$), 8 months (T = 7.981, $P < 0.001$), 10 months (T = 7.831, $P < 0.001$) and 12 months (T = 9.330, $P < 0.001$). Significant differences were also observed in the concentration of $A\beta_{42}$ between Tg mice and WT mice aged 2 months (T = 6.865, $P < 0.001$), 4

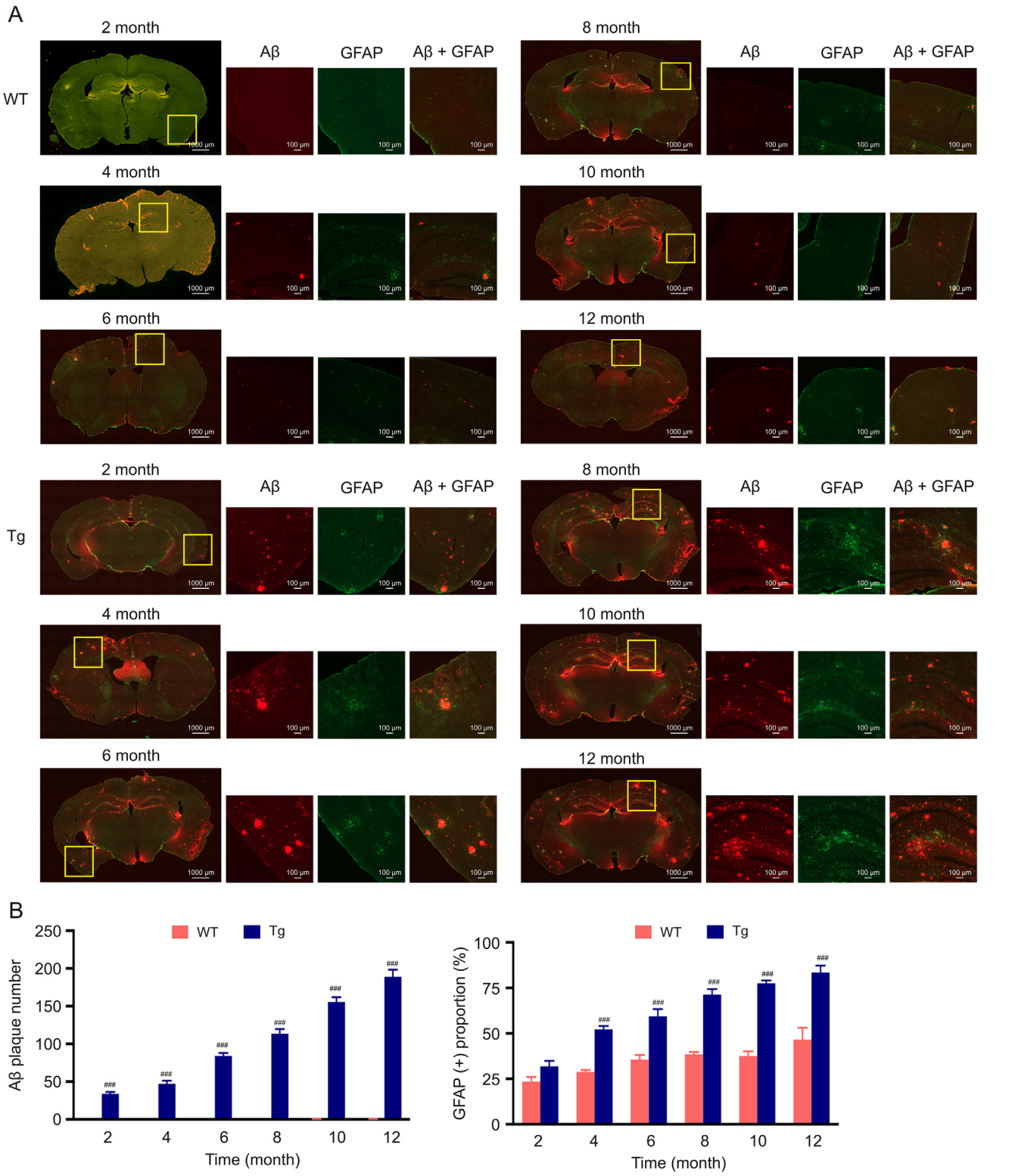

Fig. 3. Activation of astrocytes is elevated in an age-dependent manner in the brain tissues of TgCRND8 (Tg) mice. (A) Immunohistochemistry (IHC) co-staining of Aβ/GFAP in the brain tissues of Tg and wild type (WT) mice; scale bar: 50 μm. (B) Quantitative analysis of IHC staining. Data are presented as the mean ± standard error mean (SEM) ($n = 4$). $^{\#}P < 0.05$ and $^{\#\#\#}P < 0.001$ compared with the WT group (t-test).

months (T = 8.813, $P < 0.001$), 6 months (T = 12.53, $P < 0.001$), 8 months (T = 13.63, $P < 0.001$), 10 months (T = 17.78, $P < 0.001$) and 12 months (T = 17.97, $P < 0.001$) (Fig. 4A).

In addition, the concentration of TNF-α significantly differed between Tg mice and WT mice aged 2 months (T = 2.953, $P < 0.05$), 4 months (T = 3.466, $P < 0.01$), 6 months (T = 3.989, $P < 0.01$), 8 months (T = 5.722, $P < 0.001$), 10 months (T = 6.836, $P < 0.001$) and 12 months (T = 10.55, $P < 0.001$). Fig. 4B also shows significant differences in the concentration of IL-1β between Tg mice and WT mice aged 2 months (T = 3.329, $P < 0.01$), 4 months (T = 3.211,

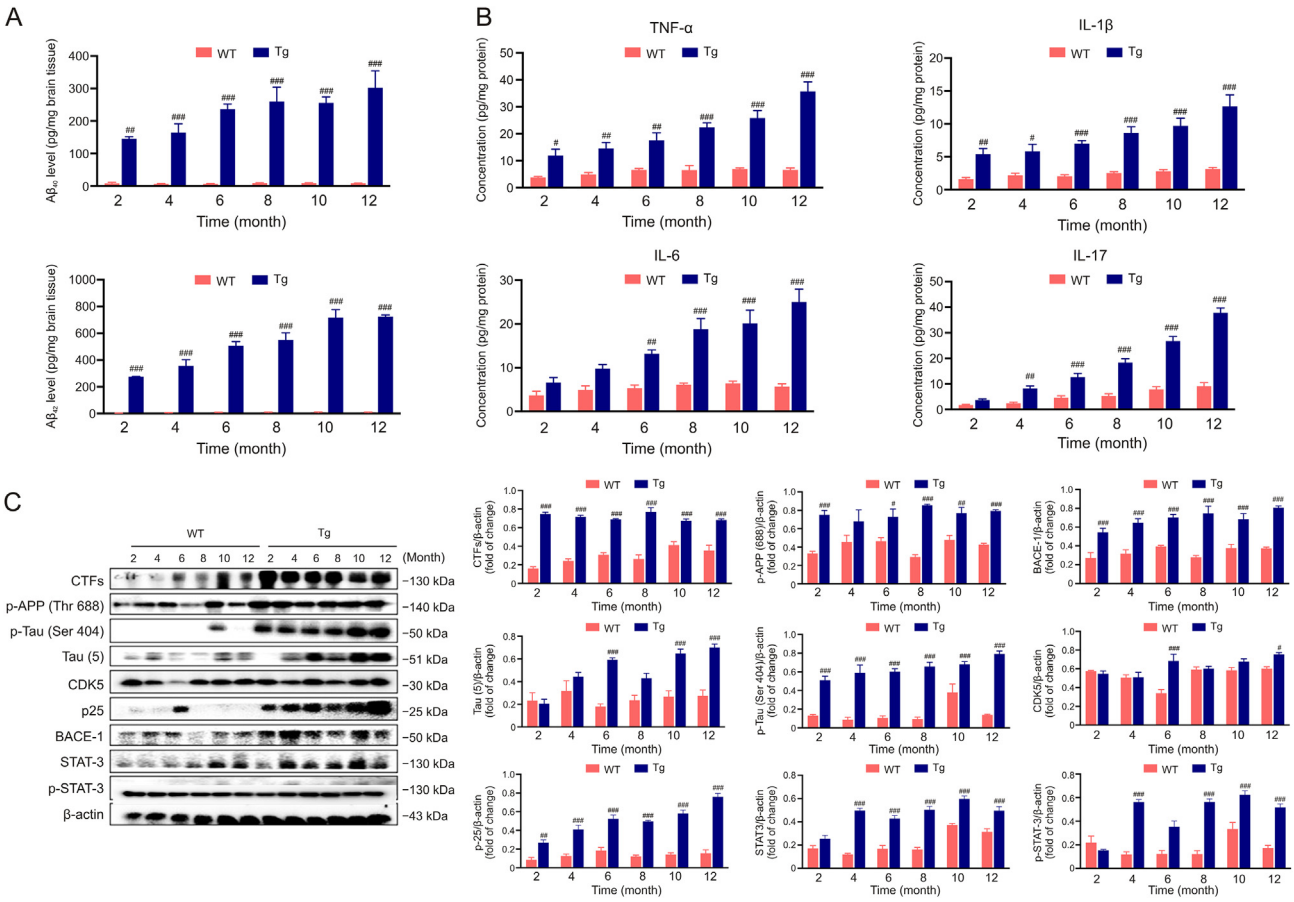

Fig. 4. Neuroinflammation is elevated in an age-dependent manner in the brain tissues of TgCRND8 (Tg) mice. (A) $A\beta_{40}$ and $A\beta_{42}$ concentrations in the brain tissues of Tg and wild-type (WT) mice. Data are presented as the mean ± standard error mean (SEM) ($n = 6$). $^{\#\#}P < 0.01$ compared with the WT group (t-test). (B) Tumor necrosis factor-α (TNF-α), interleukin-1β (IL-1β), interleukin-6 (IL-6) and IL-17 concentrations in the brain tissues of Tg and WT mice. Data are presented as the mean ± SEM ($n = 6$). $^{\#}P < 0.05$, $^{\#\#}P < 0.01$ and $^{\#\#\#}P < 0.001$ compared with the WT group (t-test). (C) Immunoblot and quantitative analysis of CTFs, p-APP (Thr 688), p-tau (Ser 404), tau (5), cyclin-dependent kinase 5 (CDK5), p25, BACE-1, transcription 3 (STAT3) and p-STAT3 in the brain tissues of Tg and WT mice. Data are presented as the mean ± SEM ($n = 3$). $^{\#}P < 0.05$, $^{\#\#}P < 0.01$ and $^{\#\#\#}P < 0.001$ compared with the WT group (t-test).

$P < 0.05$), 6 months (T = 4.325, $P < 0.001$), 8 months (T = 5.311, $P < 0.001$), 10 months (T = 6.030, $P < 0.001$) and 12 months (T = 8.320, $P < 0.001$). Further, Fig. 4B shows noticeable differences in the concentration of IL-6 between Tg mice and WT mice aged 2 months (T = 1.305, $P > 0.05$), 4 months (T = 2.193, $P > 0.05$), 6 months (T = 3.522, $P < 0.01$), 8 months (T = 5.684, $P < 0.001$), 10 months (T = 6.156, $P < 0.001$) and 12 months (T = 8.668, $P < 0.001$). Most importantly, the concentration of IL-17, which plays a critical role in incipient synaptic and cognitive changes during AD progression, was also noticeable different between Tg mice and WT mice aged 4 months (T = 3.450, $P < 0.051$), 6 months (T = 4.786, $P < 0.001$), 8 months (T = 7.824, $P < 0.001$), 10 months (T = 11.30, $P < 0.001$) and 12 months (T = 17.21, $P < 0.001$) (Fig. 4B).

Consequently, as shown in Fig. 4C, APP processing was also activated in Tg mice, as indicated by the augmented expression levels of CTFs between Tg mice and WT mice aged 2 months (T = 13.39, $P < 0.001$), 4 months (T = 10.87, $P < 0.001$), 6 months (T = 8.736, $P < 0.001$), 8 months (T = 11.56, $P < 0.001$), 10 months (T = 6.022, $P < 0.001$) and 12 months (T = 7.519, $P < 0.001$]). The protein expression of p-APP (Thr 6888) was significant between Tg mice and WT mice aged 2 months (T = 5.200, $P < 0.001$), 6 months (T = 3.298, $P < 0.05$), 8 months (T = 6.954, $P < 0.001$), 10 months (T = 3.596, $P < 0.01$) and 12 months (T = 4.547, $P < 0.001$). These findings were accompanied by the enhanced activities of p-tau (404) and tau (5), and p-tau (404) was significant differences between Tg mice and WT mice aged 2 months (T = 6.056, $P < 0.001$), 4 months (T = 8.025, $P < 0.001$], 6 months (T = 7.904, $P < 0.001$], 8 months (T = 8.955, $P < 0.001$), 10 months (T = 4.778, $P < 0.01$) and 12 months (T = 10.39, $P < 0.001$). Tau (5) was significant differences between Tg mice and WT mice aged 6 months (T = 5.992, $P < 0.001$), 10 months (T = 5.549, $P < 0.01$) and 12 months (T = 6.182, $P < 0.001$). CDK5 activation by binding to p25 is known to induce tau phosphorylation [19]. Briefly, p25/Cdk5 phosphorylates and activates the transcription factor STAT3, which positively regulates the transcription of *BACE1* gene in neuroblastoma cells; this in turn modulates APP processing [5]. As expected, both CDK5 and STAT3 expressions were significantly elevated in the brains of Tg mice relative to the age-matched WT littermates. For CDK5, significant differences were observed between Tg mice and WT mice aged 6 months (T = 6.871, $P < 0.001$) and 12 months (T = 2.975, $P < 0.05$); for STAT3, significant differences were found between Tg mice and WT mice aged 4 months (T = 10.75, $P < 0.001$), 6 months (T = 7.451, $P < 0.001$), 8 months (T = 9.704, $P < 0.001$), 10 months (T = 6.365, $P < 0.01$) and 12 months (T = 5.186, $P < 0.001$). These findings coincide with the activation of APP processing and tau phosphorylation suggested by augmented CTF and tau expression levels in Tg mice. In sum, Aβ aggregates were accompanied by detectable CDK5-mediated tau hyperphosphorylation and APP processing in the brains of Tg mice. In contrast, these signals were barely detected in the brains of WT

mice, especially in younger WT littermates. These findings suggest that CDK5/STAT3 signaling was activated in Tg mice and was positively correlated with neuroinflammation.

3.3. Gut dysbiosis occurred in Tg mice in an age-dependent manner

Studies have demonstrated a close relationship between the changes in the gut microbial community and the development of AD in mouse models [20]. However, how gut dysbiosis affects amyloid pathology in AD is still unclear. Therefore, we first explored the composition of gut microbial community in Tg mice at different ages (2, 4, 6, 8, 10 and 12 months) and in their age-matched WT littermates. As shown in Figs. 5A and B, the structures of the gut microbial community were mostly similar between Tg and WT mice at younger ages (2 and 4 months) but markedly differed at older ages (6, 8, 10 and 12 months).

Specifically, at phylum level, the gut microbiota mainly consisted of *Firmicutes, Actinobacteria*, *Proteobacteria* and *Verrucomicrobia*. The gut microbiota of Tg mice had a higher abundance of *Bacteroidetes* and a lower abundance of *Firmicutes* than that of WT mice, and marked temporal shifts were observed with advancing age, as evidenced by the dynamically altered abundances of the two predominant phyla *Firmicutes* and Bacteroidetes (Figs. 5A, 5B and S1). *Erysipelotrichi, Bacteroidia* and *Clostridia* were the major classes, representing about 80% of the gut microbial composition in WT mice. However, the abundances of the pathogenic classes *Bacilli*, *ε-Proteobacteria*, *δ-Proteobacteria* and *γ-Proteobacteria* that are closely related to the pathogenesis of AD were markedly increased in Tg mice with increasing age (Fig. S2). Furthermore, *Bifidobacteriales*, *Desulfovibrionales*, *Turicibacteriales* and *Lactobacillales* were the dominant orders in WT mice, contributing 10 strains in the gut microbiome. Compared to WT mice, Tg mice

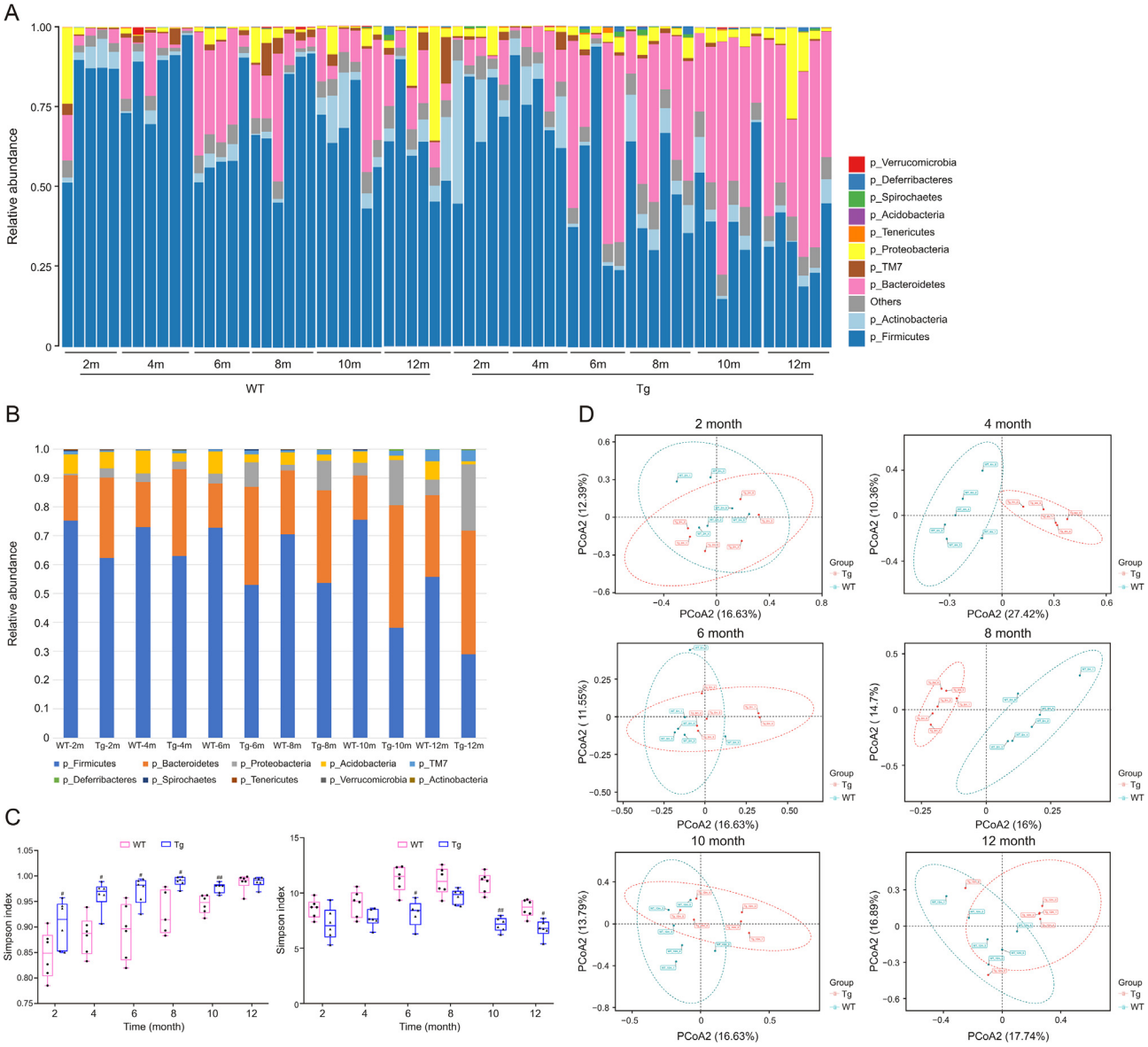

Fig. 5. Faecal microbiome analysis of TgCRND8 (Tg) mice reveals gut dysbiosis. (A) The taxonomic distribution of the faecal microbiome. (B) Relative abundance of bacterial phyla determined by high-throughput sequencing (HTS) analysis. (C) Boxplots of the α-diversity pattern including the Shannon index and Simpson index of the faecal microbiota of Tg and wild-type (WT) mice of different age groups. Data are presented as the mean ± standard error mean (SEM) ($n = 6$). $^{\#}P < 0.05$, $^{\#\#}P < 0.01$ and $^{\#\#\#}P < 0.001$ compared with the wild-type (WT) littermate group (*t*-test). (D) Principal coordinate plot (PCoA) (unweighted UniFrac method) of the faecal microbial community structure of Tg and WT mice of different age groups.

showed markedly decreased abundances of *Turicibacteriales*, *Bifidobacteriales* and *Lactobacillales* and an enhancement abundance of Desulfovibrionales (Fig. S3). At the family level, 10 families showed significantly different abundances between the gut microbial communities of Tg and WT mice (Fig. S4). The abundances of *Erysipelotrichaceae* and S24-7 were reduced, while those of *Aerococcaceae* and *Entercoccaceae* were dramatically elevated, in Tg mice compared to WT mice (Fig. S4). Finally, at genus level, the relative abundances of *Allobaculum* and *Psychrobacter* were decreased, while those of *Acinetobacter* and *Staphylococcus* were increased, in Tg mice with increasing age (Fig. S5).

The results indicated that the Simpson index was markedly enhanced, but the Shannon index was dramatically decreased, in Tg mice, indicating that the gut microbiome richness and evenness were attenuated in these mice compared with WT mice (Fig. 5C). Furthermore, the dynamic changes in the composition of the gut microbial community were visualised using a principal coordinate analysis plot based on the unweighted UniFrac method. As shown in Fig. 5D, the bacterial communities in WT mice were clustered away from those in Tg mice, indicating that the gut microbial communities changed with age in Tg mice. These findings demonstrated that gut microbiota of Tg mice had age-dependent dynamic alterations with the characteristic of a diminished microbial diversity, a temporal enrichment of pro-inflammatory *Proteobacteria* and a marked depletion in the abundance of anti-inflammatory *Firmicutes*.

The results of ANOSIM, *t*-test analysis of species differences between groups and LEfSe analysis also revealed the differences in the community structure between Tg mice and WT mice (Fig. 6). Specifically, LEfSe analysis (Fig. 6) revealed significantly increased the abundances of the *Proteobacteria* at phylum, *γ-Proteobacteria* at class, *Pseudomonadales* at order, *Moraxellaceae* at family, *Erysipelotrichales* at order and *Erysipelotrichaceae* at family in Tg mice (green nodes) relative to WT mice, indicating that these taxa played a harmful role in the cognitive function of Tg mice. Similarly, the abundances of the *Bacilli* at class, *Lactobacillaceae* at family, *Lactobacillus* at genus, *Lactobacillales* at order and *Firmicutes* at phylum (red nodes) were higher in WT mice than in Tg mice, indicating that these taxa played profitable roles in the cognitive function of WT mice.

3.4. Bioinformatics analysis of differential metabolites

In this study, the metabolic phenotype of Tg mice with AD progression at different months of age was analysed using a metabolomic approach.

As shown in Figs. 7A–C, the univariate analysis revealed prominent differences in the metabolites between Tg mice and WT mice. As shown in Fig. 8A, the multiple pattern recognition method was used for the metabolic phenotype analysis in mice of different ages. An orthogonal partial least squares discriminant analysis (OPLS-DA) model was constructed, and the parameters for model evaluation in the positive ion mode were $R^2Y = 0.97$ and $Q^2 = 0.712$. The OPLS-DA score plot revealed a clear and significant separation of metabolic phenotypes between the Tg and WT mice of different ages.

Based on the variable importance for the projection (VIP) of the OPLS-DA model, the effects of single metabolites on the classification and discrimination of each group were measured. Our study initially screened out the differences between WT group and Tg group using VIP >1 as the screening standard, and 17 different significant metabolites were identified (Table 1). Among them, Tg mice showed markedly changed levels of metabolites (high VIP values and low *P* values) involved in choline metabolism, namely, 1-palmitoyl-*sn*-glycero-3-phosphocholine, 1-stearoyl-2-hydroxy-*sn*-glycero-3-phosphocholine 1, phosphorylcholine, TMAO, PC (16:0/16:0), 1-*O*-(*cis*-9-octadecenyl)-2-*O*-acetyl-*sn*-glycero-3-phosphocholine and *N*-docosanoyl-4-sphingenyl-1-*O*-phosphorylcholine. The histogram in Fig. 8A displays the identified differential metabolites by fold change. Moreover, there was a close relationship among significant differences in metabolites (Fig. 8C). The KEGG pathway enrichment analysis of different metabolites by Fisher's exact test verified the remarkable changes observed in choline metabolism (Figs. 8B and 9). The hierarchical clustering results of the significantly different metabolites in the positive ion mode are shown in Fig. 10. The results shown in Fig. 10 are consistent with those described in Table 1.

3.5. Correlation analysis

There was a clear distinction in metabolomics and microbial diversity between WT and Tg mice, and 10 significantly different metabolites and 14 significantly different flora were screened. The correlations between these flora and metabolites were evaluated using Spearman's correlation analysis. In total, 34 significantly positive and 38 significantly negative bacteria-metabolite correlations were identified. The CytoScape and R language analysis software were used for in-depth data mining for the flora-metabolite correlations from multiple perspectives. The cluster heatmaps of Spearman's correlation hierarchical clustering analyses of remarkable differences in flora and metabolites are shown in Figs. 11 and S6. Flora in the same cluster of prominent differences in metabolites or differences at the genus level were similar to the findings of the correlation patterns. Correlations between significantly different flora and metabolites are expressed in the form of a correlation coefficient matrix heatmap in Figs. 12 and S6. The previous results revealed that the significant reductions in *Lactobacillus*, *Clostridium*, *Bifidobacterium* and *Turicibacter* in Tg mice were negatively or positively related to the expression of many lipid metabolites, including 1-palmitoyl-*sn*-glycero-3-phosphocholine, TMAO, PC(16:0/16:0), 1-*O*-(*cis*-9-octadecenyl)-2-*O*-acetyl-*sn*-glycero-3-phosphocholine, *N*-docosanoyl-4-sphingenyl-1-*O*-phosphorylcholine and 1-stearoyl-2-arachidonoyl-*sn*-glycerol, between WT and Tg mice aged 6, 8, 10 and 12 months (Figs. 11, 12, S6, S7, S8 and S9 and Table 2).

3.6. WT-FMT treatment alleviated cognitive deficits and AD pathology in Tg mice

The results of the MWMT indicated that the cognitive deficits in Tg mice with FMT from aged WT donors (hereafter WT-FMT-treated mice) were clearly improved but those with FMT from aged Tg donors (hereafter Tg-FMT-treated mice) were worsened (Fig. 13B). There was a dominant difference in the mean latency during the training stage between training days ($F(3, 112) = 30.50$, $P < 0.001$) and treatments ($F(3, 112) = 17.40$, $P < 0.001$), but no interaction effect was found between treatments and training days ($F(6, 112) = 0.1802$, $P > 0.05$). Notably, Tg-FMT-treated mice spent longer to find the platform during the training period than WT-FMT-treated mice (day 1, $F(3, 28) = 2.984$, $P < 0.05$; day 2, $F(3, 28) = 5.789$, $P < 0.01$; day 3, $F(3, 28) = 3.951$, $P < 0.05$; day 4, $F(3, 28) = 5.377$, $P < 0.01$). In addition, Tg-FMT-treated mice showed more obvious deficits in spatial memory, indicating by spending less time in target quadrant ($F(3, 28) = 11.32$, $P < 0.001$) and fewer crossings of the target quadrant which had a hidden platform ($F(3, 28) = 18.02$, $P < 0.001$) than WT-FMT-treated mice in the probe test. The results of OFT demonstrated that the time spent in the central area ($F(3, 28) = 3.969$, $P < 0.05$) and total distance travelled ($F(3, 28) = 3.969$, $P < 0.05$) were prominent more in WT-FMT-treated mice than in Tg-FMT-treated mice, indicating that the anxiety and motor functions were improved in the former mice (Fig. 13C), while cognitive and mobility deficits were exacerbated in the latter.

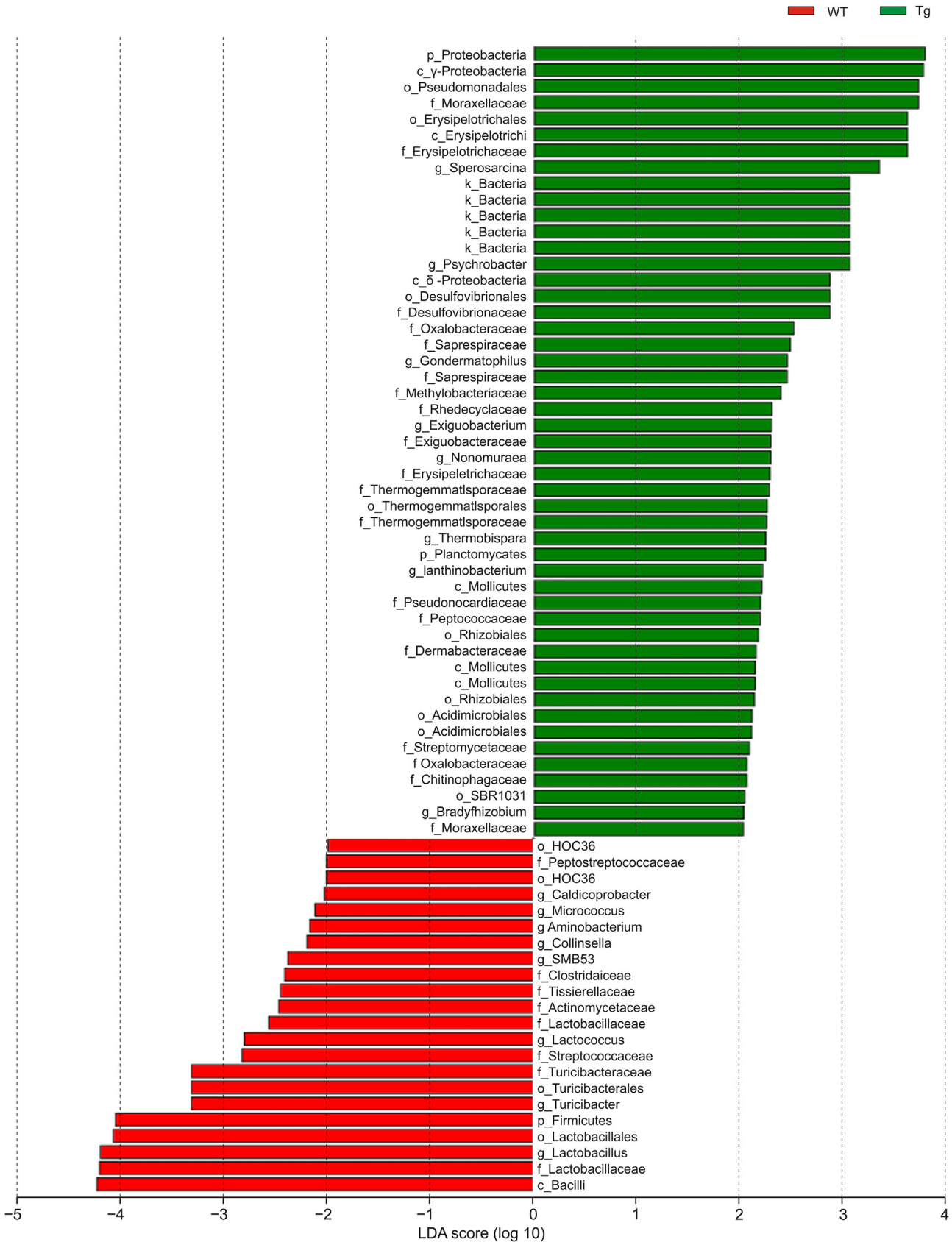

Fig. 6. Metabolomic analysis of the plasma samples of TgCRND8 (Tg) mice of different ages using linear discriminant analysis effect size (LEfSe).

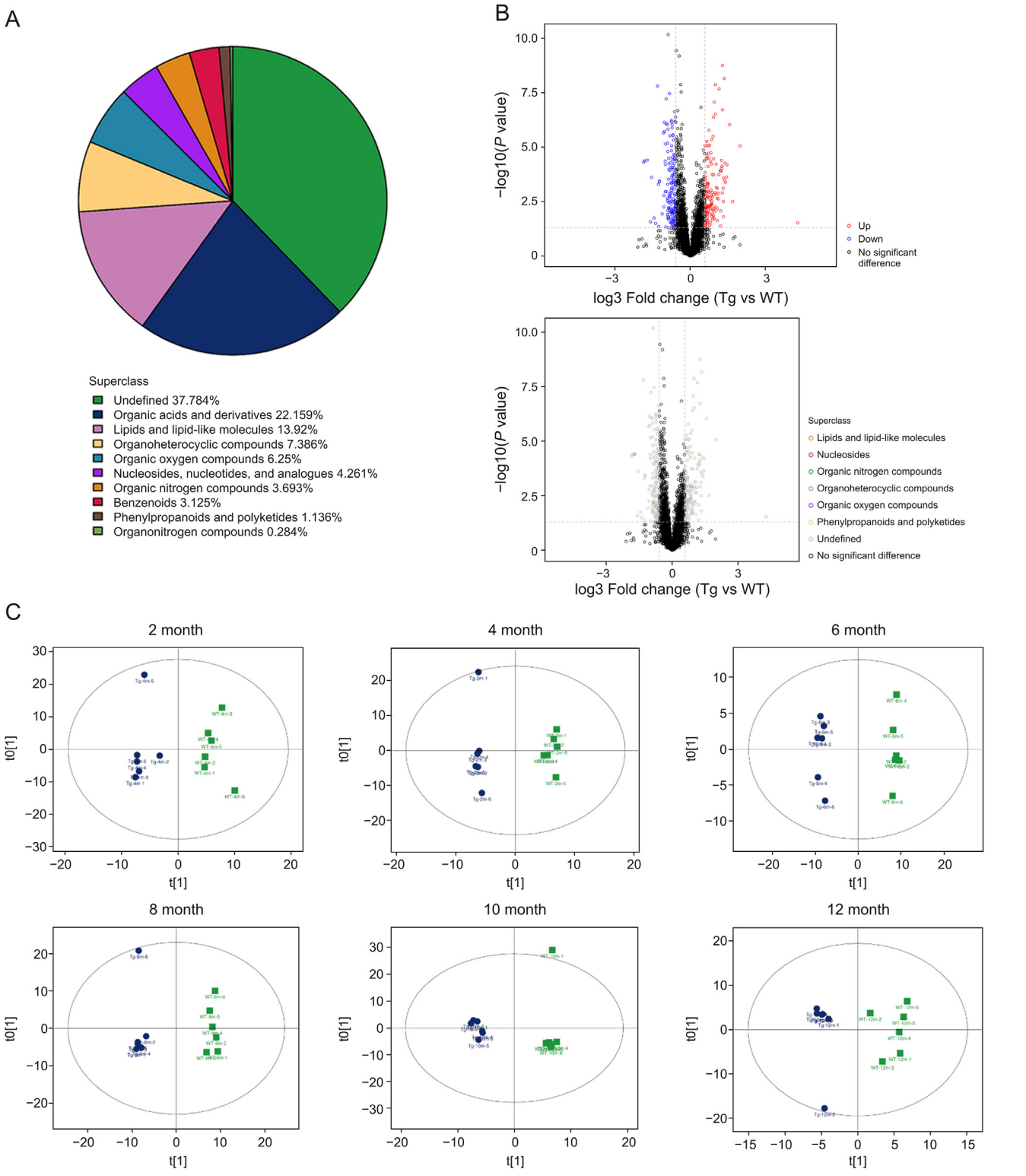

Fig. 7. Bioinformatics analysis of TgCRND8 (Tg) mice reveals changes in differential metabolites. (A) Classification of the determined metabolites. (B) Volcano plot in the positive ion mode, in which the red dot indicates fold change >1.5 and $P < 0.05$ indicates the differential metabolites identified using univariate statistical analysis. (C) Orthogonal partial least squares discriminant analysis (OPLS-DA) score plot in the positive ion mode. Green dots represent the wild-type (WT) samples, while blue dots represent the Tg group.

The concentrations of neuroinflammatory biomarkers, namely, TNF-α, IL-6 and IL-17, were prominently decreased in the brain ($F(3, 23) = 18.02$, $P < 0.001$; $F(3, 23) = 17.71$, $P < 0.001$; and $F(3, 20) = 12.87$, $P < 0.001$; respectively) and colon ($F(3, 24) = 37.62$, $P < 0.001$; $F(3, 24) = 20.16$, $P < 0.001$; and $F(3, 20) = 11.07$, $P < 0.001$; respectively) tissues of WT-FMT-treated mice relative to Tg-FMT-treated mice (Figs. 13D–F). As shown in Fig. 14B, the concentrations of TMAO in both brain ($F(3, 21) = 8.553$, $P < 0.001$) and colon ($F(3, 22) = 7.293$, $P < 0.001$) tissues were prominently elevated in Tg mice. After WT-FMT treatment, the concentrations

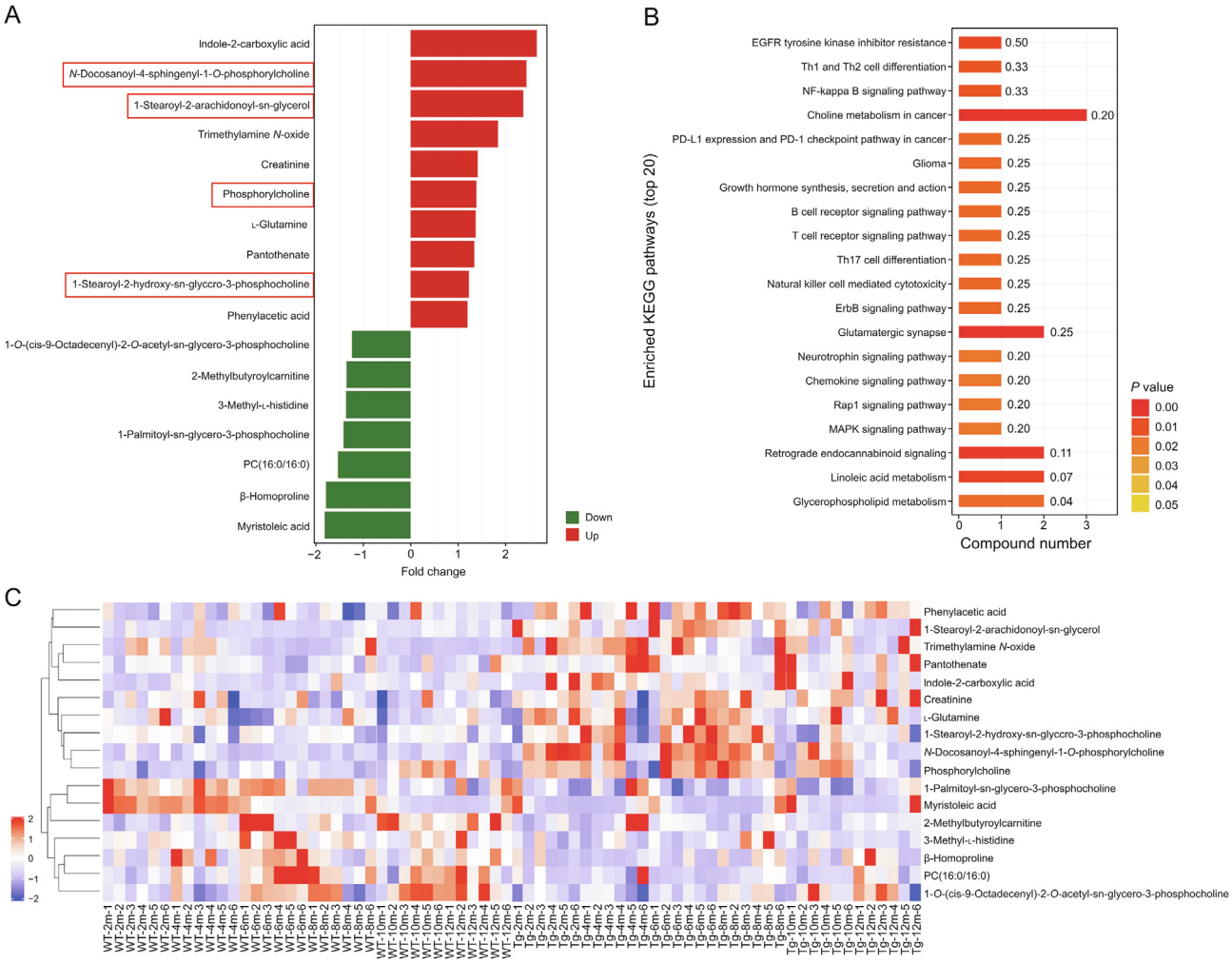

Fig. 8. Bioinformatics analysis of TgCRND8 (Tg) mice reveals changes in differential metabolites. (A) Kyoto Encyclopedia of Genes and Genomes (KEGG) pathway enrichment analysis of differentially expressed metabolites showed significant alterations in choline metabolism. (B) Differential metabolites in choline metabolism. (C) A heat-map displaying the correlations among differential metabolites involved in choline metabolism in Tg mice.

of TMAO in the brain ($P < 0.05$) and colon ($P < 0.001$) tissues were prominently reduced, whereas Tg-FMT treatment could not effectively inhibit TMAO production in the brain and colon tissues of Tg mice.

IHC staining revealed that the expression levels of IBA-1 ($F(3, 16) = 16.65$, $P < 0.001$), GFAP ($F(3, 16) = 36.07$, $P < 0.001$) and Aβ ($F(3, 12) = 62.23$, $P < 0.001$) were elevated in the brains of Tg mice (Fig. 13C). Consistently, the concentrations of $A\beta_{40}$ ($F(3, 23) = 109.9$,

Table 1
Identification of significantly differential metabolites in plasma of TgCRND8 and wild type (WT) mice (positive ion mode).

Metabolite	Formula	*m/z*	ID	VIP	Pathway
1-Palmitoyl-sn-glycero-3-phosphocholine	$C_{24}H_{50}NO_7P$	496.34	HMDB0010382	32.14	Choline metabolism
1-Stearoyl-2-hydroxy-sn-glycero-3-phosphocholine	$C_{26}H_{54}NO_7P$	524.37	HMDB0010384	21.17	Choline metabolism
Phosphorylcholine	$C_5H_{15}NO_4P$	184.07	HMDB0001565	6.33	Choline metabolism
Trimethylamine *N*-oxide	C_3H_9NO	76.08	HMDB0000925	2.71	Choline metabolism
PC (16:0/16:0)	$C_{40}H_{80}NO_8P$	756.55	HMDB0000564	2.6	Choline metabolism
1-O-(*cis*-9-Octadecenyl)-2-O-acetyl-sn-glycero-3-phosphocholine	–	550.38	–	2.07	Choline metabolism
N-Docosanoyl-4-sphingenyl-1-O-phosphorylcholine	–	809.65	–	2.1	Choline metabolism
Creatinine	$C_4H_7N_3O$	114.07	HMDB0000562	2.64	Creatinine phosphate
1-Stearoyl-2-arachidonoyl-sn-glycerol	$C_{41}H_{72}O_5$	627.53	HMDB0007170	2.52	Phosphatidylcholine biosynthesis
3-Methyl-L-histidine	$C_7H_{11}N_3O_2$	170.09	HMDB0000479	2.56	Histinine metabolism
Phenylacetic acid	$C_8H_8O_2$	119.05	HMDB0000209	1.16	Phenylacetate metabolism
Indole-2-carboxylic acid	$C_9H_7NO_2$	162.05	HMDB0002285	1.12	Inhibitor of lipid peroxidation
Pantothenate	$C_9H_{17}NO_5$	220.12	HMDB0000210	1.1	Vitamin B5
Myristoleic acid	$C_{14}H_{26}O_2$	209.19	HMDB0002000	1.69	Fatty acid metabolism
β-Homoproline	$C_6H_{11}NO_2$	130.09	HMDB0029444	1.36	Organic compounds
L-Glutamine	$C_5H_{10}N_2O_3$	188.1	HMDB0000641	1.96	Phenylacetate metabolism
2-Methylbutyroylcarnitine	$C_{12}H_{23}NO_4$	246.1	HMDB0000378	1.47	Fatty acid metabolism

The metabolites with significance difference orthogonal partial least squares discriminant analysis (OPLS-DA), variable importance for the projection (VIP) > 1 and *P* value < 0.05 were listed.

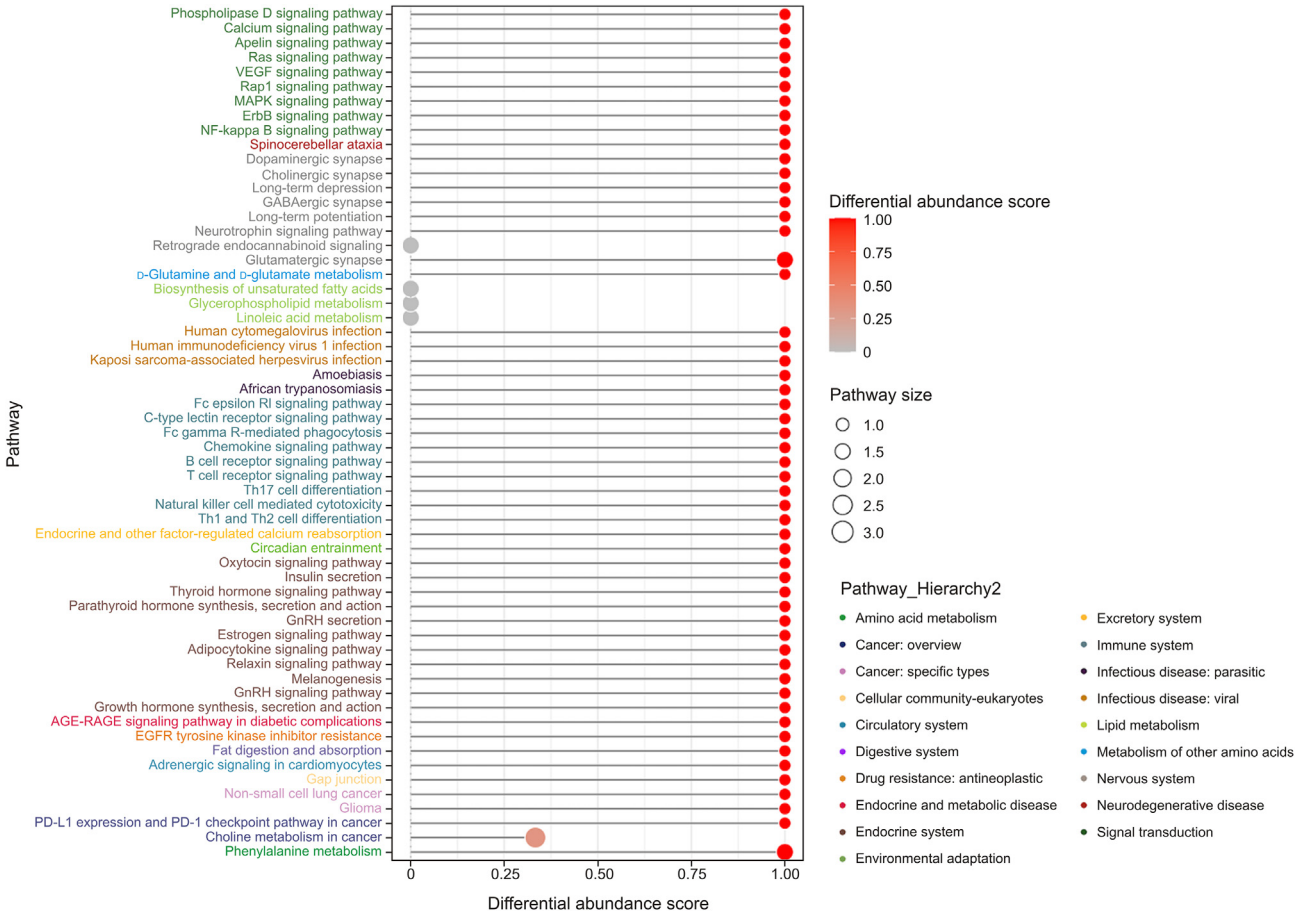

Fig. 9. Differential pathways with abundance scores screened in TgCRND8 (Tg) mice. Larger circles indicate significantly greater effects of choline metabolism (the second line from the bottom).

$P < 0.001$) and $A\beta_{42}$ ($F(3, 22) = 29.20$, $P < 0.001$) in Tg mice were also exacerbated (Fig. 13A). The results of Aβ staining and the concentrations of $A\beta_{40}$ ($P < 0.05$) and $A\beta_{42}$ ($P < 0.01$) demonstrated that accumulated Aβ fibrils were significantly attenuated by WT-FMT treatment (Figs. 14A and C). As shown in Fig. 14C, positive signals of IBA-1 in microglia and GFAP in astrocytes were dominantly reduced ($P < 0.05$ and $P < 0.01$, respectively) upon WT-FMT treatment.

Immunoblotting analysis of brain lysates from Tg mice revealed elevated levels of the full-length APP recognised by *N*-terminal (CTF) antibody ($F(3, 8) = 76.44$, $P < 0.001$), demonstrating the activation of APP processing. Notably, p-tau (Thr 205) and p-tau (Ser 404), the two major phosphorylated forms of tau, indicated that tau hyperphosphorylation was substantially mitigated in the brains of WT-FMT-treated Tg mice (both $P < 0.001$) (Fig. 14D). Consequently, the downstream substrates of APP cleavage were markedly reduced upon WT-FMT treatment, leading to a reduction in BACE-1 expression. WT-FMT treatment further attenuated the levels of both CDK5 and p-STAT-3/STAT-3, resulting in the reduction of APP production (Fig. 14D). These findings indicate that WT-FMT treatment attenuated the CDK5/STAT-3 signaling pathway and inhibited amyloid pathology in Tg mice, thereby improving cognitive functions in the mice.

3.7. Excessive choline treatment aggravated cognitive deficits and AD pathology in Tg mice

Choline metabolism plays a pivotal role in the progression of AD. To verify the role of choline metabolism in AD, we administered excessive choline to Tg mice. As shown in Fig. 15B, the cognitive deficits in Tg mice were clearly accelerated after overdose choline treatment. There was a prominent difference in the mean latency during the training stage between training days ($F(3, 84) = 52.02$, $P < 0.001$) and treatments ($F(2, 84) = 43.46$, $P < 0.001$), while no interaction effect was found between training days and treatments ($F(6, 84) = 0.146$, $P > 0.05$). However, Tg mice spent longer to seek the platform during the training period than WT mice (day 1, $F(2, 21) = 3.878$, $P < 0.05$; day 2, $F(2, 21) = 4.185$, $P < 0.05$; day 3, $F(2, 21) = 10.816$, $P < 0.01$; day 4, $F(2, 21) = 15.637$, $P < 0.01$). In addition, Tg mice showed more obvious deficits in spatial memory function, by spending less time in the target quadrant ($F(2, 21) = 11.32$, $P < 0.001$) and fewer crossings of the target quadrant ($F(2, 21) = 18.02$, $P < 0.001$) than WT mice in the probe test. Notably, excessive choline-treated Tg mice took longer to find the hidden platform on day 4 ($P < 0.05$) in the training stage than Tg vehicle-treated mice. In the OFT, the time spent in the central area ($F(2, 18) = 6.670$, $P < 0.001$) and total distance travelled ($F(2, 21) = 8.490$, $P < 0.001$) were decreased in excessive choline-treated Tg mice compared with Tg vehicle-treated mice, indicating that the anxiety and mobility deficits in Tg mice were deteriorated by excessive choline treatment (Fig. 15C).

Excessive choline supplementation also exacerbated neuroinflammation in Tg mice. As expected, TNF-α and IL-6 concentrations were progressively increased in the brain ($F(2, 18) = 6.670$, $P < 0.001$ and $F(2, 15) = 75.74$, $P < 0.001$, respectively) and colon ($F(2, 15) = 27.32$, $P < 0.001$ and $F(2, 15) = 5.917$, $P < 0.05$, respectively) tissues of Tg mice relative to WT mice, and excessive

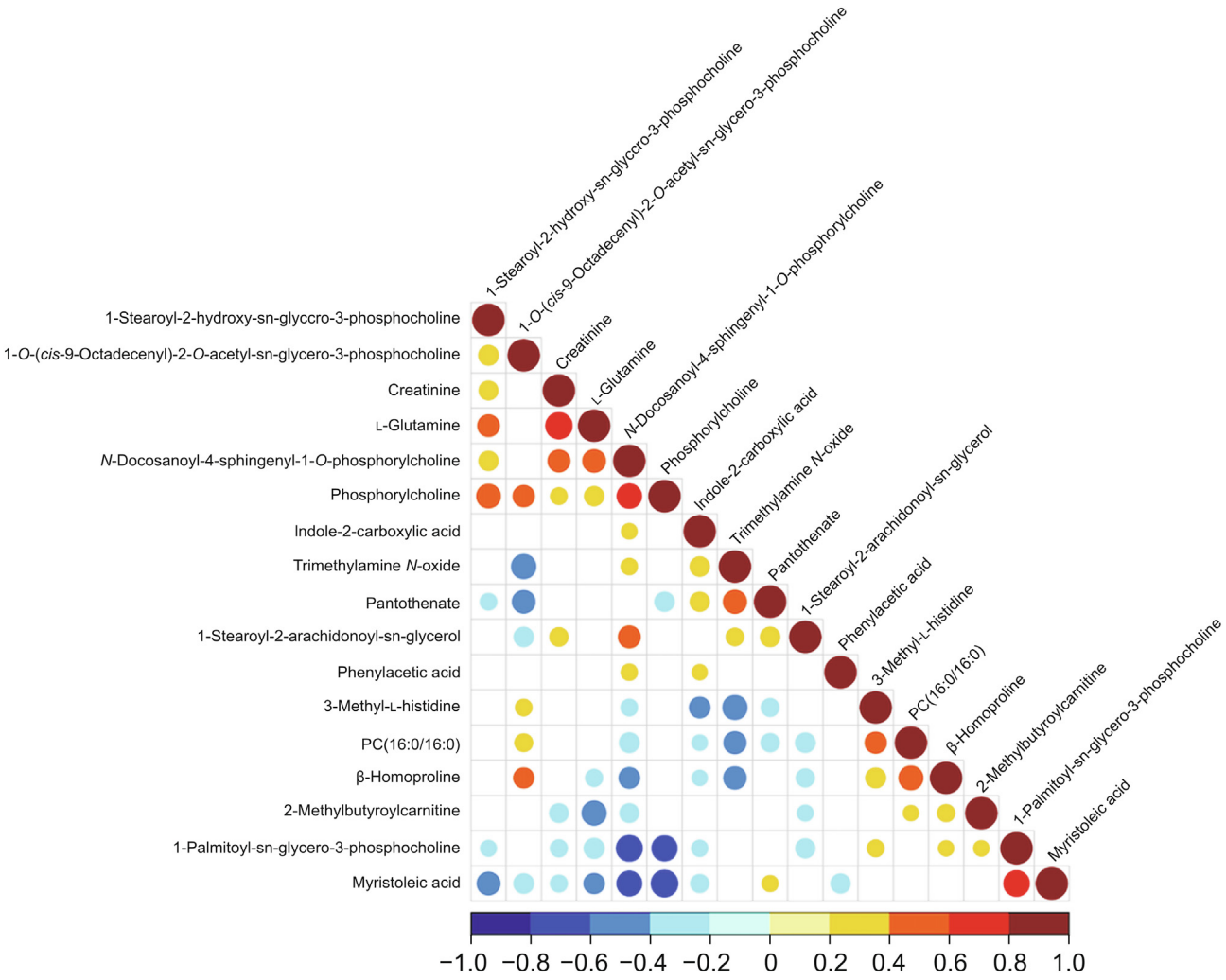

Fig. 10. Correlation heatmap of differential metabolites of TgCRND8 (Tg) mice obtained in the positive ion mode.

choline treatment further increased the concentrations of TNF-α and IL-6 relative to vehicle treatment (Figs. 15D and E). The concentrations of $A\beta_{40}$ ($F(2, 15) = 44.34$, $P < 0.001$) and $A\beta_{42}$ ($F(2, 15) = 31.64$, $P < 0.001$) were remarkably higher in Tg mice than in those of WT mice (Fig. 15F), and excessive choline supplementation further significantly increased the concentration of $A\beta_{42}$ ($P < 0.05$) in brain tissues compared with vehicle treatment. IHC staining results of Aβ and the concentrations of $A\beta_{40}$ and $A\beta_{42}$ demonstrated that Aβ deposition was significantly enhanced by excessive choline supplementation treatment (Fig. 15G). IBA-1 and GFAP ($P < 0.01$) signals in the brain tissues were markedly enhanced by excessive choline supplementation. Aβ signals in the brains were also markedly increased ($F(2, 6) = 160.3$, $P < 0.001$), indicating that excessive choline supplementation significantly enhanced Aβ production (Fig. 15G). Furthermore, we used western blotting analysis to investigate whether the activation of the CDK5/STAT3 signaling pathway in the brain by excessive choline treatment involves any other mechanisms. As shown in Fig. 15H, the expression levels of p-tau (Ser 404) were significantly elevated in the brain tissues of Tg mice ($F(2, 6) = 78.45$, $P < 0.001$) compared with WT mice. Excessive choline treatment didn't display any notable effect on the tau (5) protein levels in Tg mice. In addition, compared with WT mice, the expression levels of BACE-1 were markedly elevated ($F(2, 6) = 36.61$, $P < 0.001$) in the brain tissues of the Tg mice, while those of CDK5, p-25 ($F(2, 6) = 8.618$, $P < 0.05$), STAT3 ($F(2, 6) = 25.76$, $P < 0.01$) and p-STAT3 ($F(2, 6) = 6.967$, $P < 0.05$) were marginally increased. Excessive choline treatment further significantly enhanced the expressions of p-25 and STAT3 (both $P < 0.05$) and marginally elevated those of BACE-1.

4. Discussion

It's well-accepted that there is a functional crosstalk between gut microbiota, microbe-derived metabolites and brain function through microbiota-gut-brain axis [21]. We herein speculate that gut dysbiosis facilitates gut microbe-derived metabolite production to exacerbate AD progression through a pro-inflammatory state. In this study, the age-dependently dynamic changes in the gut microbiota composition of Tg mice were strongly correlated with the cognitive dysfunction during AD progression. FMT from Tg mice notably exacerbated cognitive deficits and neuroinflammation in Tg mice, while these changes were greatly improved by FMT from WT mice. Also, we found that choline mechanism was abnormal in Tg mice and that excessive choline treatment aggravated the cognitive deficits in Tg mice. These observations collectively highlight the functional linkage between the gut, neuroinflammation, and brain functions during AD progression.

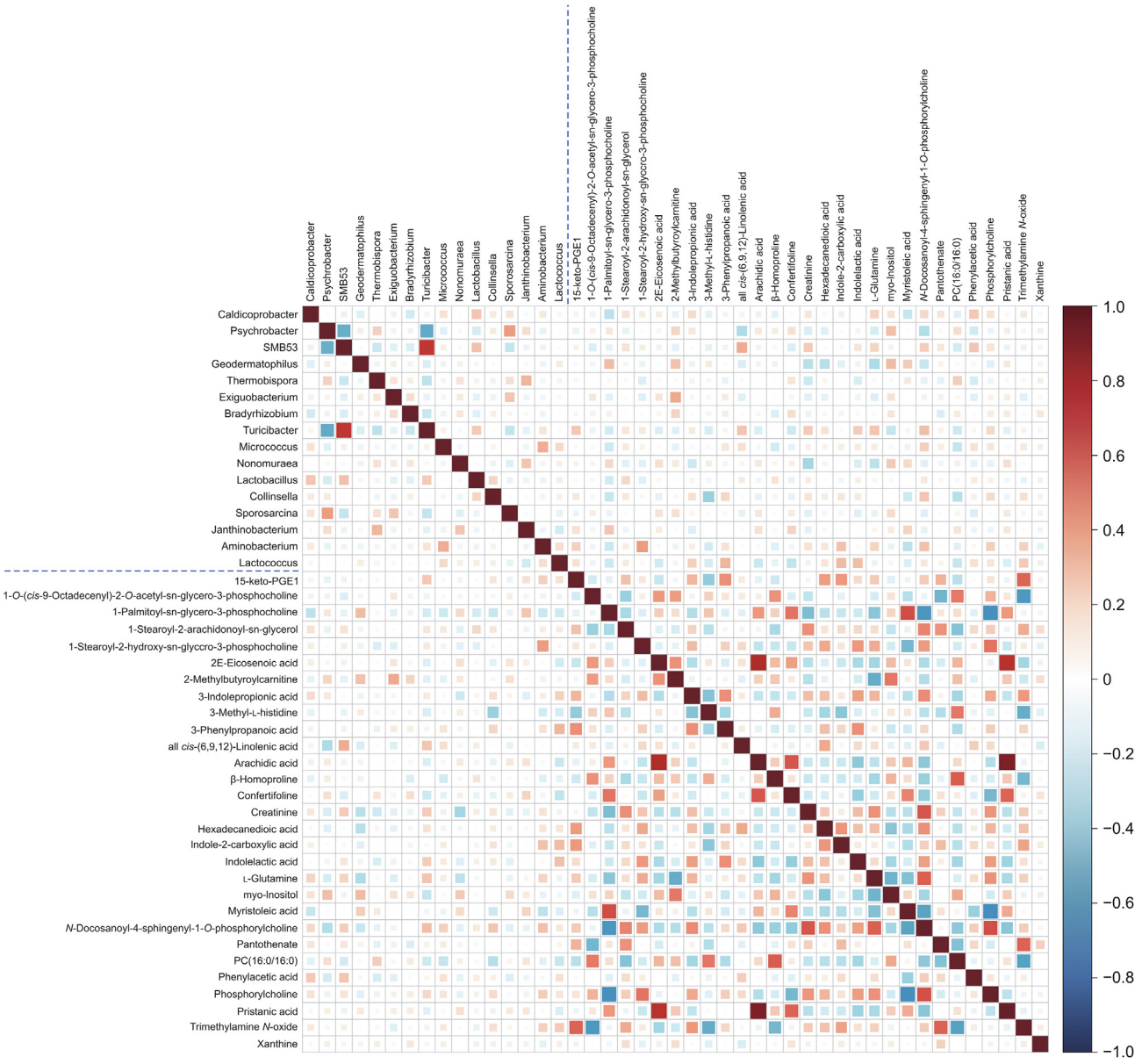

Fig. 11. Correlation coefficient matrix heat map of significantly different gut flora and metabolites between wild-type (WT) and TgCRND8 (Tg) mice.

There is no doubt that neuroinflammation can trigger Aβ pathology in the progression of AD. Overproduction of pro-inflammatory cytokines activated the first line of brain defence microglia and astrocytes, resulting in the production of reactive oxygen species (ROS), increased the accumulation of neuropathological hallmarks, which in turn initiated and aggravated neuroinflammation in the CNS [22–24]. In our study, the levels of TNF-α, IL-1β, IL-6 and IL-17 were significantly elevated in Tg mice age-dependently when compared with WT mice. IL-17 plays a critical role in early synaptic/cognitive changes during AD progression [25]. Besides, the abnormally activated microglia and astrocytes in Tg mice suggested extensive neuro-inflammation and severe damage of the blood-brain barrier (BBB) [26]. Then the disrupted BBB enables the participation of the gut microbiome in the progress of neuroinflammation, resulting in enhance of the production of pro-inflammatory cytokines and increase in gut permeability [27]. It's a vicious cycle that finally aggravates AD progression.

On the other hand, 95% of the symbiotic microbes of humans are located in the gut and play an irreplaceable role in inflammation, immunity, neurotrophy, and protection against the infections of pathogens. Gut dysbiosis is strongly related to a reduction in phylogenetic richness, especially in diseases that are characterised by intestinal inflammation and damaged gastrointestinal barrier integrity, such as AD [28]. Our results indicated that the composition and diversity of the gut microbiota deteriorated in Tg mice with advancing age, which indicated potential intestinal inflammation and impaired gastrointestinal barrier integrity. Some abundant microbiota at phyla level in the gut such as *Proteobacteria* and *Bacteroidetes* are pathogenic and participate in the pro-inflammatory process, while the phylum *Firmicutes* and family *Lactobacillaceae* exert anti-inflammatory activity. In AD patients, the relative abundances of *Lachnospiraceae*, *Bacteroidaceae*, *Veillonellaceae*, *Negativicutes* and *Bacteroidia* are markedly decreased, while those of *Ruminococcaceae*, *Lactobacillaceae*, *Actinobacteria* and *Bacilli* are increased [21]. These alterations of the gut microbiota composition

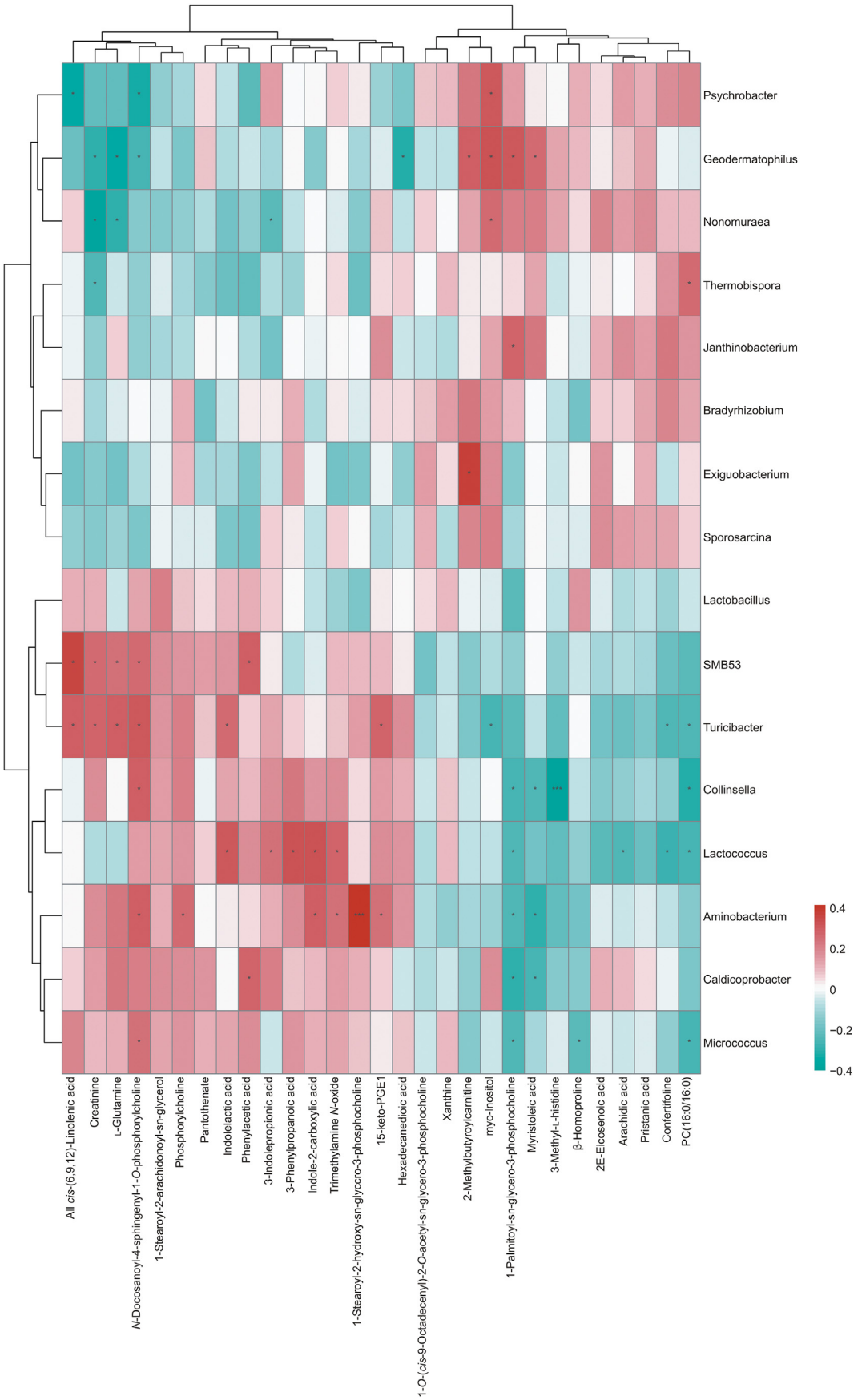

Fig. 12. Cluster heat map of spearman's correlation hierarchical clustering analysis of significant differences in gut flora and metabolites.

Table 2
Correlation between differential metabolites of choline metabolism and microbiota at different months of TgCRND8 mice.

Differential metabolites/strain	*Adlercreutzia*	*Clostridium*	SMB53	*Facklamia*	*Bifidobacteriu*	*Akkermansia*	Sychrobacter	*Kaistobacter*	*Turicibacter*
1-Palmitoyl-sn-glycero-3-phosphocholine		Negative* (8 month)* $R = 0.626^{*}$; $P = 0.0293^{*}$			Negative* (6 month)* $R = 0.706^{*}$; $P = 0.0102^{*}$	Negative* (8 month)* $R = 0.656^{*}$; $P = 0.0205^{*}$	Positive# (8 month)# $R = 0.631^{\#}$ $P = 0.0277^{\#}$		
Phosphorylcholine						Positive# (8 month)# $R = 0.578^{\#}$; $P = 0.0492^{\#}$		Positive# (8 month)# $R = 0.585^{\#}$; $P = 0.0459^{\#}$	
TMAO	Negative* (6 month)* $R = 0.769^{*}$; $P = 0.0345^{*}$								
PC (16:0/16:0)		Negative* (8 month)* $R = 0.733^{*}$; $P = 0.0666^{*}$	Negative* (10 month)* $R = 0.729^{*}$; $P = 0.072^{*}$				Positive# (8 month)# $R = 0.781^{\#}$; $P = 0.00272^{\#}$		Negative* (10 month)* $R = 0.685^{*}$; $P = 0.0139^{*}$
1-O-(*cis*-9-Octadecenyl)-2-O-acetyl-sn-glycero-3-phosphocholine					Negative* (6 month)* $R = 0.727^{*}$; $P = 0.0736^{*}$				
N-Docosanoyl-4-sphingenyl-1-O-phosphorylcholine		Positive# (8 month)# $R = 0.591^{\#}$; $P = 0.0431^{\#}$				Positive# (8 month)# $R = 0.688^{\#}$; $P = 0.0134^{\#}$			
1-Stearoyl-2-arachidonoyl-sn-glycerol	Negative* (6 month)* $R = 0.636^{*}$; $P = 0.0261^{*}$			Negative* (10 month)* $R = 0.658^{*}$; $P = 0.0199^{*}$			Negative* (8 month)* $R = 0.599^{*}$; $P = 0.0396^{*}$		Positive# (10 month)# $R = 0.608^{\#}$; $P = 0.0358^{\#}$

* represents negative relationship between differential genus and metabolites; # represents positive relationship between differential genus and metabolites.
TMAO: trimethylamine *N*-oxide; PC: phenylacetic acid.

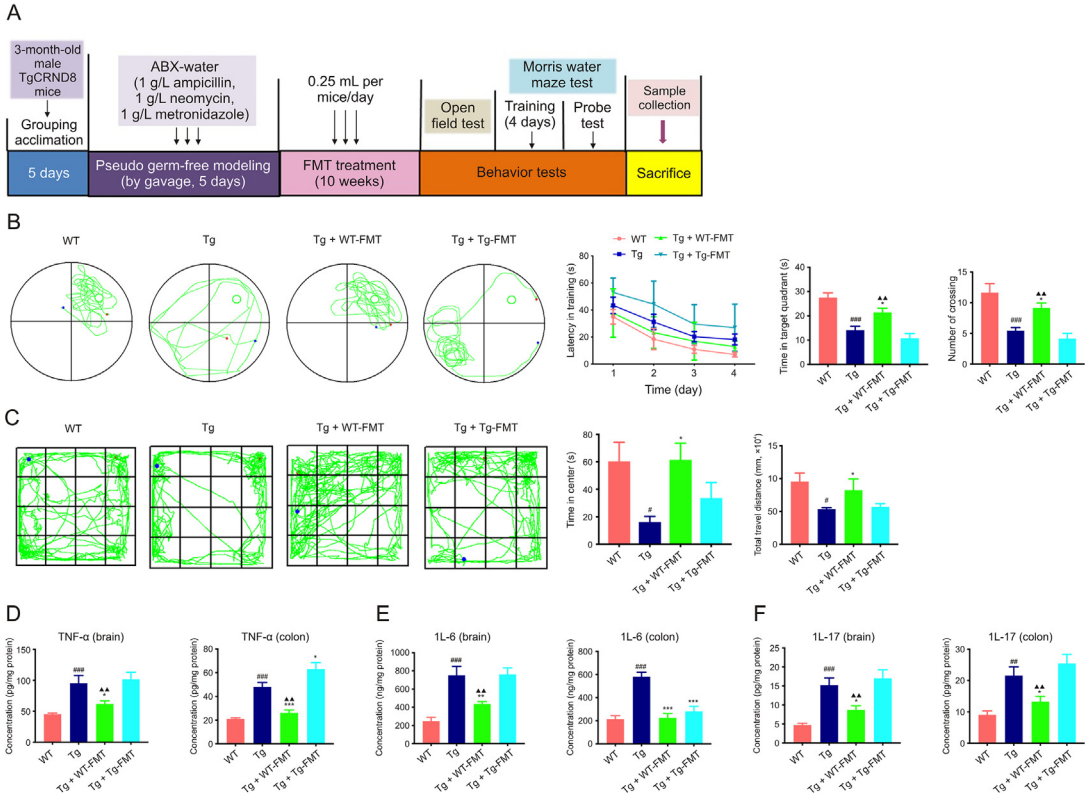

Fig. 13. Wild-type mice-faecal microbiota transplantation (WT-FMT) treatment alleviates cognitive deficits and inflammatory response in TgCRND8 (Tg) mice. (A) Schematic diagram of the protocol design ($n = 8$). (B) Escape latency of mice for 4 consecutive training days, frequency of mice crossing the platform, time spent in the target quadrant and representative swimming tracks of mice in the Morris water maze task (MWMT). Data are presented as the mean ± standard error mean (SEM) ($n = 8$). (C) Time spent in the central area, total distance travelled and representative swimming tracks of mice in MWMT. Data are presented as the mean ± SEM ($n = 8$). (D–F) The tumor necrosis factor-α (TNF-α), interleukin-6 (IL-6), and IL-17 concentrations in the brain and colon tissues of mice. Data are presented as the mean ± SEM ($n = 6$). $^{\#}P < 0.05$, $^{\#\#}P < 0.01$ and $^{\#\#\#}P < 0.001$ compared with the WT group; $^{*}P < 0.05$, $^{**}P < 0.01$ and $^{***}P < 0.001$ compared with the Tg + vehicle group; $^{▲▲}P < 0.01$ compared with the Tg + Tg-FMT group (one-way ANOVA).

facilitated the leakage of gut bacteria and their metabolites into the body circle. Consistent with these reports [21], *Proteobacteria* and *Bacteroidetes* were found to be highly enriched in the gut microbiome of Tg mice in the present study. A decreased *Firmicutes*/*Bacteroidetes* ratio is considered to play a critical role in neuroprotection in AD patients [29]. Furthermore, at the genus level, the abundances of *Staphylococcus* and Acinetobacter were increased (by 2.6-fold) in 4-month-old Tg mice compared to WT mice of similar age. Increased abundances of *Staphylococcus* in the gut microbiome have also been found to be linked to AD progression [30]. In this study, we discovered that FMT from Tg mice accelerated the neuroinflammation and cognitive dysfunction in Tg mice, while that from WT mice improved cognitive deficits, indicating gut microbiota exerts a pivotal role in AD progression.

Even so, the mechanistic interaction between gut dysbiosis and neuro-inflammation in AD remains vague. But the neurotransmitters, organic acids and amino acids that were generated by gut microbiota, were found to be altered in plasma and urine samples of patients with brain disorders [31]. Therefore, it's assumed that the metabolic pathways of these gut microbe-derived metabolites exert a major role in these CNS diseases [32,33]. Notably, TMAO, a gut microbe-derived metabolite involved in choline metabolism, has been proven as a novel prognostic marker in cardiovascular disease [34,35] and found to play potential role in several chronic diseases like diabetes [36,37]. Other studies have proved that increased TMAO may exacerbate cognitive deficits and brain aging to speed up neurodegeneration [38,39], suggesting its strong involvement in AD pathology. TMAO level has also been identified to be enhanced in the cerebrospinal fluid of AD patients compared with healthy individuals [40]. Given these recent reports, TMAO has been considered to be a promising AD biomarker. Our results indicated that the composition of metabolites was markedly altered in AD mice. The most dominant change appeared in the metabolites involved in the choline-related pathway. Also, we proved that the TMAO concentration was significantly elevated in the blood of AD mice. These findings further corroborate the TMAO overproduction by the gut microbiota could promote choline-mediated neuroinflammation in AD.

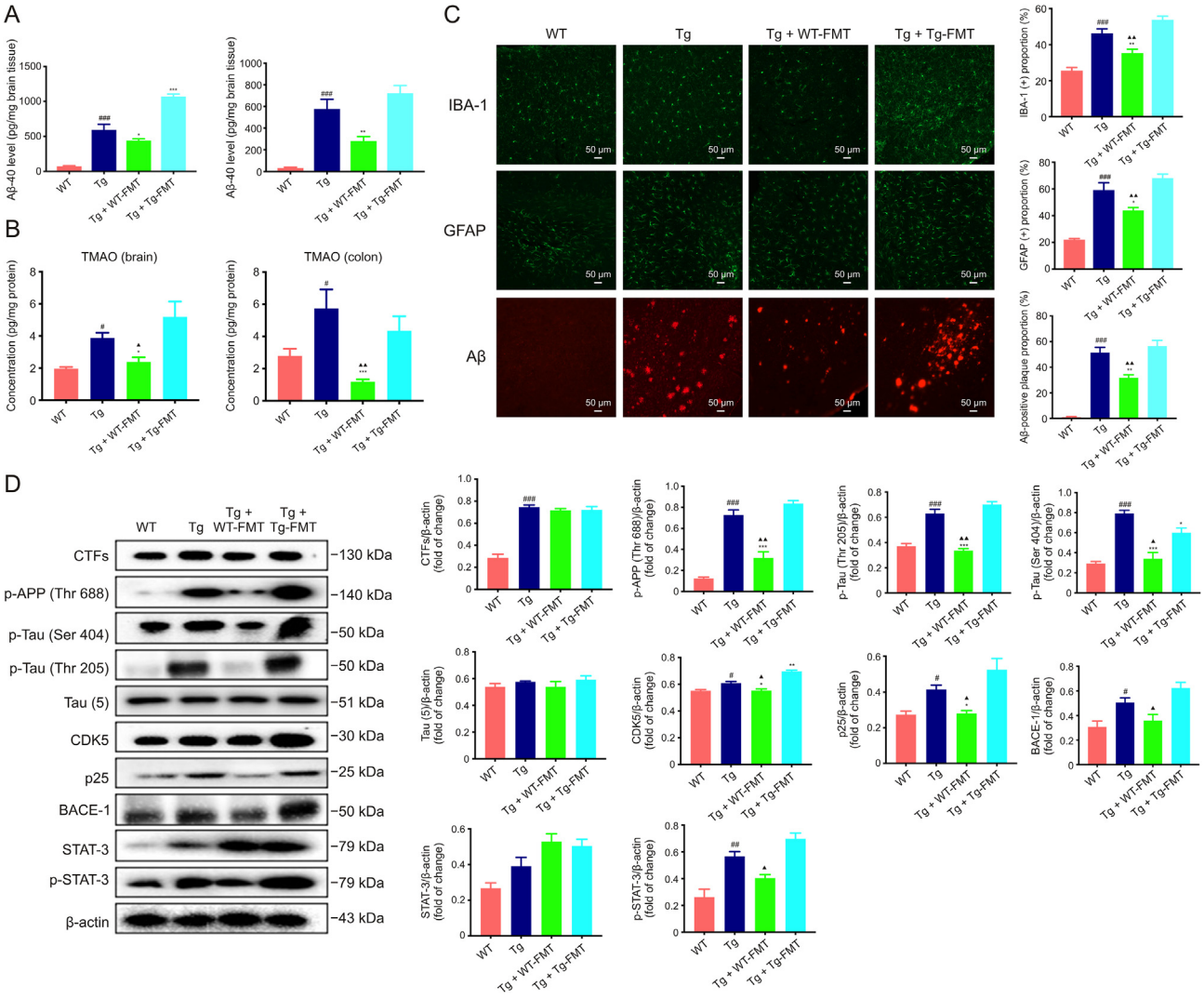

Fig. 14. Wild-type mice-faecal microbiota transplantation (WT-FMT) treatment alleviates Alzheimer's disease (AD) pathology in TgCRND8 (Tg) mice. (A) $A\beta_{40}$ and $A\beta_{42}$ concentrations in the brain tissues of mice. Data are presented as the mean ± standard error mean (SEM) ($n = 6$). (B) Trimethylamine *N*-oxide (TMAO) concentrations in the colon and brain tissues of mice. Data are presented as the mean ± SEM ($n = 6$). (C) IBA-1, GFAP and Aβ staining in the brain sections of mice, and quantitative analysis of IBA-1-positive microglia, GFAP-positive astrocytes and Aβ-positive plaque. Scale bar: 50 μm. Data are presented as the mean ± SEM ($n = 4$). (D) Immunobloting and quantitative analysis of CTFs, p-APP (Thr 688), p-tau (Thr 205), p-tau (Ser 404), tau (5), CDK5, p25, BACE-1, STAT3, and p-STAT3 in the brain tissues of mice. Data are presented as the mean ± SEM ($n = 3$). $^{\#}P < 0.05$, $^{\#\#}P < 0.01$ and $^{\#\#\#}P < 0.001$ compared with the WT group; $^{*}P < 0.05$, $^{**}P < 0.01$ and $^{***}P < 0.01$ compared with the Tg + vehicle group; $^{\blacktriangle}P < 0.05$ and $^{\blacktriangle\blacktriangle}P < 0.01$ compared with the Tg + Tg-FMT group (one-way ANOVA).

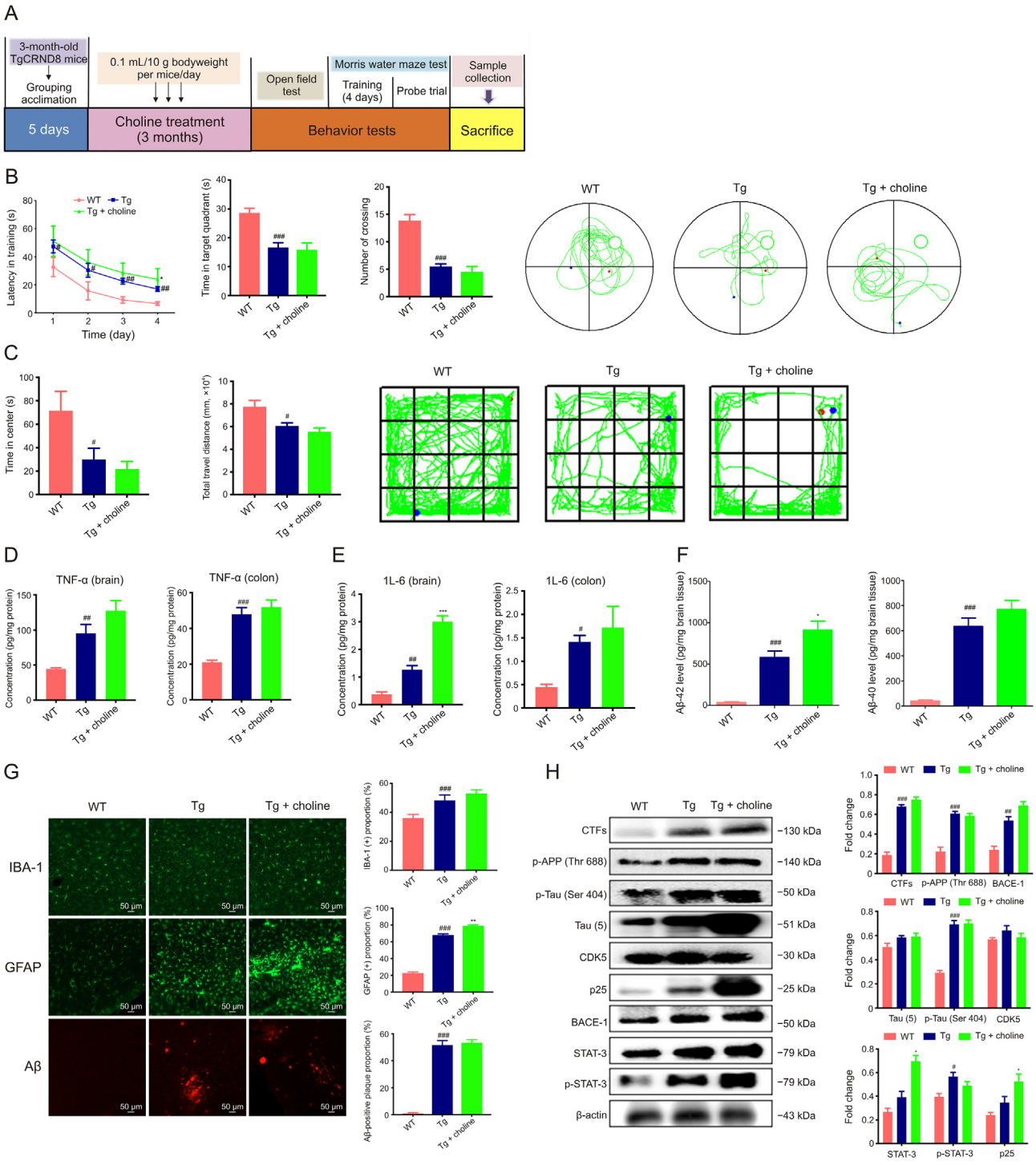

Fig. 15. Excessive choline treatment aggravates cognitive deficits and Alzheimer's disease (AD) pathology in TgCRND8 (Tg) mice. (A) Schematic diagram of the protocol design ($n = 8$). (B) Escape latency of mice for 4 consecutive training days, frequency of mice crossing the platform, time spent in the target quadrant and representative swimming tracks of mice in the Morris water maze task (MWMT). Data are presented as the mean ± standard error mean (SEM) ($n = 8$). (C) Time spent in the central area, total distance travelled and representative swimming tracks of mice in the open field test (OFT). Data are presented as the mean ± SEM ($n = 8$). (D–E) Tumor necrosis factor-α (TNF-α), and interleukin-6 (IL-6) concentrations in the brain and colon tissues of Tg mice. Data are presented as the mean ± SEM ($n = 6$). (F) $A\beta_{40}$ and $A\beta_{42}$ concentrations in the brain tissues of mice. Data are presented as the mean ± SEM ($n = 6$). (G) Trimethylamine *N*-oxide (TMAO) concentration in the brain tissues of mice. Data are presented as the mean ± SEM ($n = 6$). (H) IBA-1, GFAP and Aβ staining in the brain tissues of the Tg mice and quantitative analysis of IBA-1-positive microglia, GFAP-positive astrocytes and Aβ-positive plaque. Scale bar: 50 μm. Data are presented as the mean ± SEM ($n = 4$). (I) Immunoblotting and quantitative analysis of CTFs, p-APP (Thr 688), p-tau (Thr 205), p-tau (Ser 404), tau (5), CDK5, p25, BACE-1, STAT3, and p-STAT3 in the brain tissues of mice. Data are presented as the mean ± SEM ($n = 3$). $^{\#}P < 0.05$, $^{\#\#}P < 0.01$ and $^{\#\#\#}P < 0.001$ compared with the wild-type (WT) group; $^{*}P < 0.05$, $^{**}P < 0.01$ compared with the Tg vehicle-treated group.

As mentioned above, abnormal choline metabolism was found in Tg mice in this study. Actually, choline is an essential nutrient, similar to indispensable amino acids, vitamins, fatty acids and minerals. The Food and Nutrition Board of the Institute of Medicine of the National Academy of Sciences (USA) recommends a mean daily intake of 7.5 mg/kg body weight of choline [41]. Lower choline consumption in adult humans may cause liver dysfunction, muscle damage and other pathological symptoms [41–43]. However, excessive choline administration also exerts adverse effects. High consumption of choline has been reported to accelerate the oxidation of trimethylamine to TMAO by the gut microbiota in the liver, and abnormal TMAO level conduces to AD pathogenesis [44]. Indeed, higher TMAO level was found in the cerebrospinal fluid of AD patients than in healthy individuals [40]. Furthermore, elevated circulating TMAO levels have been shown to reduce hippocampal antioxidant enzyme levels [45].

In this study, excessive choline treatment in mice was equivalent to 15 times the recommended daily choline dose for human adults. This treatment resulted in declined cognitive functions and elevated TMAO level in Tg mice. Our findings collectively highlight that as a driver factor, gut microbiota may promote certain metabolites that are closely related to neuroinflammation in AD progression. Afterward, we discovered higher concentrations of TMAO in both the brain and colon tissues of Tg mice, which was consistent with the previous conclusion.

Although CDK5/STAT3 pathway activation has been found to play a key role in AD development, the relationship between the CDK5/STAT3 pathway and gut dysbiosis has not been clearly understood. In our present study, Tg-FMT treatment elevated the expression of CDK5, while Tg-WT treatment suppressed the expression of CDK5, p25 and p-STAT3 in the brain tissues of Tg mice, indicating that gut dysbiosis may induce CDK5/STAT3 pathway activation in Tg mice. Moreover, excessive choline treatment elevated the expression of p25, BACE-1, p-STAT3 and STAT3 in the brain tissues of Tg mice. Our findings shed light on the interaction between gut dysbiosis or excessive choline treatment and the CDK5/STAT3 signaling pathway activation.

5. Conclusions

Our study demonstrated that gut dysbiosis occurred in Tg mice in an age-dependent manner, altered choline metabolism in the host and activated CDK5/STAT3 pathway in the brain. Moreover, FMT treatments from aged Tg mice even exacerbated AD pathology, enhanced choline metabolism and promoted the activation of CDK5/STAT3 pathway in Tg mice, which were suppressed by FMT from WT littermates. Furthermore, excessive choline treatment declined cognitive functions and accelerated neuroinflammation in Tg mice. In a word, these findings highlight that as a driving factor, gut dysbiosis accelerates gut microbe-derived metabolite production, which in turn promotes AD progression. The involving microbiota-gut-brain axis mechanisms underlying AD pathology revealed in this study may afford a new perspective on the novel targets for AD treatment.

CRediT author statement

Chang Qu: Methodology, Validation, Formal analysis, Investigation, Data curation, Writing - Original draft preparation; **Qing-Qing Xu:** Investigation; **Wen Yang:** Data curation; **Mei Zhong:** Formal analysis; **Qiuju Yuan:** Resources; **Yan-Fang Xian:** Conceptualization, Methodology, Writing - Original draft preparation, Reviewing and Editing, Supervision, Funding acquisition; **Zhi-Xiu Lin:** Conceptualization, Writing - Reviewing and Editing, Supervision.

Declaration of competing interest

The authors declare that there are no conflicts of interest.

Acknowledgments

This work was partially supported by National Natural Science Foundation of China (Project No.: 82104414), Natural Science Foundation of Guangdong Province of China (Project No.: 2022A1515011682) and a direct grant from The Chinese University of Hong Kong (Project No.: 2021.071).

Appendix A. Supplementary data

Supplementary data to this article can be found online at https://doi.org/10.1016/j.jpha.2023.07.014.

References

[1] H.W. Querfurth, F.M. LaFerla, Alzheimer's disease, N Engl J. Med. 362 (2010) 329–344.
[2] T.D. McKee, R.M. Loureiro, J.A. Dumin, et al., An improved cell-based method for determining the γ-secretase enzyme activity against both Notch and APP substrates, J. Neurosci. Meth. 213 (2013) 14–21.
[3] S. Liu, C. Wang, T. Jiang, et al., The role of Cdk5 in Alzheimer's disease, Mol. Neurobiol. 53 (2016) 4328–4342.
[4] T. Lu, C. Wan, W. Yang, et al., Role of Cdk5 in amyloid-beta pathology of Alzheimer's disease, Curr. Alzheimer Res. 16 (2019) 1206–1215.
[5] Y. Wen, E. Planel, M. Herman, et al., Interplay between cyclin-dependent kinase 5 and glycogen synthase kinase 3 beta mediated by neuregulin signaling leads to differential effects on tau phosphorylation and amyloid precursor protein processing, J. Neurosci. 28 (2008) 2624–2632.
[6] A.K. Fu, W.Y. Fu, A.K. Ng, et al., Cyclin-dependent kinase 5 phosphorylates signal transducer and activator of transcription 3 and regulates its transcriptional activity, Proc. Natl. Acad. Sci. U. S. A. 101 (2004) 6728–6733.
[7] J. Wan, A.K. Fu, F.C. Ip, et al., Tyk2/STAT3 signaling mediates beta-amyloid-induced neuronal cell death: Implications in Alzheimer's disease, J. Neurosci. 30 (2010) 6873–6881.
[8] X. Hu, T. Wang, F. Jin, Alzheimer's disease and gut microbiota, Sci. China Life Sci. 59 (2016) 1006–1023.
[9] N.M. Vogt, R.L. Kerby, K.A. Dill-McFarland, et al., Gut microbiome alterations in Alzheimer's disease, Sci. Rep. 7 (2017), 13537.
[10] P. Tognini, Gut microbiota: A potential regulator of neurodevelopment, Front. Cell. Neurosci. 11 (2017), 25.
[11] Q.-Q. Xu, W. Yang, M. Zhong, et al., Animal models of Alzheimer's disease: Preclinical insights and challenges, Acta Mater. Med. 2 (2023) 192–215.
[12] H. Li, S.P. Ip, Q. Yuan, et al., Isorhynchophylline ameliorates cognitive impairment via modulating amyloid pathology, tau hyperphosphorylation and neuroinflammation: Studies in a transgenic mouse model of Alzheimer's disease, Brain Behav. Immun. 82 (2019) 264–278.
[13] C. Qu, Q. Li, Z. Su, et al., Nano-Honokiol ameliorates the cognitive deficits in TgCRND8 mice of Alzheimer's disease via inhibiting neuropathology and modulating gut microbiota, J. Adv. Res. 35 (2022) 231–243.
[14] Q. Xu, Z. Su, W. Yang, et al., Patchouli alcohol attenuates the cognitive deficits in a transgenic mouse model of Alzheimer's disease via modulating neuropathology and gut microbiota through suppressing C/EBPβ/AEP pathway, J. Neuroinflammation 20 (2023), 19.
[15] L. Zhao, Y. Huang, L. Lu, et al., Saturated long-chain fatty acid-producing bacteria contribute to enhanced colonic motility in rats, Microbiome 6 (2018), 107.
[16] Q. Wang, Y. Shen, X. Wang, et al., Concomitant memantine and *Lactobacillus plantarum* treatment attenuates cognitive impairments in APP/PS1 mice, Aging 12 (2020) 628–649.
[17] Y. Xian, S.P. Ip, H. Li, et al., Isorhynchophylline exerts antidepressant-like effects in mice *via* modulating neuroinflammation and neurotrophins: Involvement of the PI3K/Akt/GSK-3β signaling pathway, FASEB J 33 (2019) 10393–10408.
[18] Y. Xian, D. Fan, S.P. Ip, et al., Antidepressant-like effect of isorhynchophylline in mice, Neurochem. Res. 42 (2017) 678–685.
[19] J.C. Cruz, H.C. Tseng, J.A. Goldman, et al., Aberrant Cdk5 activation by p25 triggers pathological events leading to neurodegeneration and neurofibrillary tangles, Neuron 40 (2003) 471–483.
[20] C. Chen, E.H. Ahn, S.S. Kang, et al., Gut dysbiosis contributes to amyloid pathology, associated with C/EBPβ/AEP signaling activation in Alzheimer's disease mouse model, Sci. Adv. 6 (2020), eaba0466.
[21] P. Liu, G. Peng, N. Zhang, et al., Crosstalk between the gut microbiota and the brain: An update on neuroimaging findings, Front. Neurol. 10 (2019), 883.
[22] W. Chen, X. Zhang, W. Huang, Role of neuroinflammation in neurodegenerative diseases (review), Mol. Med. Rep. 13 (2016) 3391–3396.

[23] I. Morales, L. Guzmán-Martínez, C. Cerda-Troncoso, et al., Neuroinflammation in the pathogenesis of Alzheimer's disease. A rational framework for the search of novel therapeutic approaches, Front. Cell. Neurosci. 8 (2014) 112.
[24] J.W. Kinney, S.M. Bemiller, A.S. Murtishaw, et al., Inflammation as a central mechanism in Alzheimer's disease, Alzheimers Dement 4 (2018) 575–590.
[25] H.C. Brigas, M. Ribeiro, J.E. Coelho, et al., IL-17 triggers the onset of cognitive and synaptic deficits in early stages of Alzheimer's disease, Cell Rep 36 (2021), 109574.
[26] H. Akiyama, S. Barger, S. Barnum, et al., Inflammation and Alzheimer's disease, Neurobiol. Aging 21 (2000) 383–421.
[27] F. Pistollato, S.S. Cano, I. Elio, et al., Role of gut microbiota and nutrients in amyloid formation and pathogenesis of Alzheimer disease, Nutr. Rev. 74 (2016) 624–634.
[28] S. Liu, J. Gao, M. Zhu, et al., Gut microbiota and dysbiosis in Alzheimer's disease: Implications for pathogenesis and treatment, Mol. Neurobiol. 57 (2020) 5026–5043.
[29] T. Doifode, V.V. Giridharan, J.S. Generoso, et al., The impact of the microbiota-gut-brain axis on Alzheimer's disease pathophysiology, Pharmacol. Res. 164 (2021), 105314.
[30] S. Westfall, D.M. Dinh, G.M. Pasinetti, Investigation of potential brain microbiome in Alzheimer's disease: Implications of study bias, J. Alzheimers Dis. 75 (2020) 559–570.
[31] J.F. Cryan, K.J. O'Riordan, C.S.M. Cowan, et al., The microbiota-gut-brain axis, Physiol. Rev. 99 (2019) 1877–2013.
[32] S. Isaiah, D.T. Loots, R. Solomons, et al., Overview of brain-to-gut axis exposed to chronic CNS bacterial infection(s) and a predictive urinary metabolic profile of a brain infected by *Mycobacterium tuberculosis*, Front. Neurosci. 14 (2020), 296.
[33] Z. Wang, E. Klipfell, B.J. Bennett, et al., Gut flora metabolism of phosphatidylcholine promotes cardiovascular disease, Nature 472 (2011) 57–63.
[34] C. Roncal, E. Martínez-Aguilar, J. Orbe, et al., Trimethylamine-N-oxide (TMAO) predicts cardiovascular mortality in peripheral artery disease, Sci. Rep. 9 (2019), 15580.
[35] M. Dambrova, G. Latkovskis, J. Kuka, et al., Diabetes is associated with higher trimethylamine N-oxide plasma levels 124 (2016) 251–256.
[36] C.W.H. Chan, B.M.H. Law, M.M.Y. Waye, et al., Trimethylamine-N-oxide as one hypothetical link for the relationship between intestinal microbiota and cancer - where we are and where shall we go? J. Cancer 10 (2019) 5874–5882.
[37] R. Xu, Q. Wang, Towards understanding brain-gut-microbiome connections in Alzheimer's disease, BMC Syst. Biol. 10 (Suppl 3) (2016), 63.
[38] Q. Ma, C. Xing, W. Long, et al., Impact of microbiota on central nervous system and neurological diseases: The gut-brain axis, J. Neuroinflammation 16 (2019), 53.
[39] D. Li, Y. Ke, R. Zhan, et al., Trimethylamine-N-oxide promotes brain aging and cognitive impairment in mice, Aging Cell 17 (2018), e12768.
[40] N.M. Vogt, K.A. Romano, B.F. Darst, et al., The gut microbiota-derived metabolite trimethylamine N-oxide is elevated in Alzheimer's disease, Alzheimers. Res. Ther. 10 (2018), 124.
[41] Food, Nutrition Board, Dietary Reference Intakes for Thiamin, Riboflavin, Niacin, Vitamin B6, Folate, Vitamin B12, Panthotenic Acid, Biotin, and Cholin, National Academy Press, Washington, 1998.
[42] S.C. Garner, M.H. Mar, S.H. Zeisel, Choline distribution and metabolism in pregnant rats and fetuses are influenced by the choline content of the maternal diet, J. Nutr. 125 (1995) 2851–2858.
[43] S.H. Zeisel, K.A. da Costa, P.D. Franklin, et al., Choline, an essential nutrient for humans, FASEB J 5 (1991) 2093–2098.
[44] K.A. da Costa, M. Badea, L.M. Fischer, et al., Elevated serum creatine phosphokinase in choline-deficient humans: Mechanistic studies in C2C12 mouse myoblasts, Am. J. Clin. Nutr. 80 (2004) 163–170.
[45] K.A. da Costa, M.D. Niculescu, C.N. Craciunescu, et al., Choline deficiency increases lymphocyte apoptosis and DNA damage in humans, Am. J. Clin. Nutr. 84 (2006) 88–94.